Effects of Doxorubicin on the Functional Activity of $Na_V1.5$ Voltage-gated Sodium Channels in a Breast Carcinoma Cell Line

Robert Allen

MSc by Research

University of York

Biology

December 2022

Table of Contents

List of Tables and Figures

List of Abbreviations

CAM – Cell Adhesion Molecule
CaMKII – Ca^{2+}/Calmodulin-dependent Kinase II
C_m – Cell Membrane Capacitance
CNS – Central Nervous System
CPA – Cyclopiazonic Acid
DMEM – Dulbecco's Modified Eagle Medium
ER – Endoplasmic Reticulum
FCS – Foetal Calf Serum
HER2 – Human Epidermal Growth Factor Receptor 2
I/V – Current/Voltage relationship
K – Slope Factor
NCX – Na^+/Ca^{2+} exchanger
NHE1 – Na^+/H^+ exchanger
OD – Absorbance- Optical Density
oER – Oestrogen Receptor
PD – Pore Domain
PNS – Peripheral Nervous system
PSS – Physiological Saline Solution
PR – Progesterone Receptor
RNS – Reactive Nitrogen Species
ROS – Reactive Oxygen Species
RyR – Ryanodine Receptor
SF – Selectivity Filter
SR – Sarcoplasmic Reticulum
τ_f – Fast Time Constant of Inactivation
Tp – Time to Current Peak
TNBC – Triple Negative Breast Cancer
TRPC – Transient Receptor Potential Channel
τ_s – Slow Time Constant of Inactivation
TTX – Tetrodotoxin
$V_{1/2}$ activation/inactivation – Voltage at Half Activation/Inactivation
Va – Voltage of Activation
VGSC – Voltage-gated Sodium Channel
V_m – Membrane Potential
Vp – Voltage at Current Peak

1. Abstract

The anthracycline drug doxorubicin, commonly used in treatment of triple negative breast cancers, has been shown to cause cardiac toxicity at high doses. This is as a result of indirect modulation of $Na_v1.5$ voltage-gated sodium channels in cardiomyocytes, resulting in an increased persistent Na^+ current via a Ca^{2+}/calmodulin-dependent protein kinase II (CaMKII) dependent mechanism. $Na_v1.5$ is also expressed in breast cancer cells, where its activity promotes tumour migration and invasion. The possibility that doxorubicin could promote these behaviours via increased $Na_v1.5$ function in breast cancer cells has not been explored.

The aim of this study was to investigate the effect of doxorubicin on the persistent Na^+ current carried by $Na_v1.5$ in the metastatic triple-negative breast cancer cell line MDA-MB-231 and the mechanism behind any changes. We used whole-cell patch clamp recording to assess Na^+ currents in voltage clamp mode. We also used the ratiometric Ca^{2+} indicator Fura-2 to evaluate changes in Ca^{2+} homeostasis in response to doxorubicin treatment.

We found that both acute application and 2-hour pre-treatment with 5 μM doxorubicin significantly increased the mean persistent Na^+ current in MDA-MB-231 cells. The use of inhibitors of CaMKII, Ca^{2+} signalling and reactive oxygen species (ROS) did not significantly prevent this increase in persistent Na^+ current, although trends in the data suggest that CaMKII and ROS have roles in the mechanism. Ca^{2+} imaging experiments revealed no measurable increase in cytosolic Ca^{2+} concentration in response to acute application of 5 μM doxorubicin and pre-treatment with doxorubicin did not significantly affect Ca^{2+} levels in the intracellular stores. Ptychographic experiments showed an overall decrease in motility in response to doxorubicin, although clusters of cells showed resistance to treatment.

We conclude that doxorubicin treatment increases persistent Na^+ current in breast cancer cells expressing $Na_v1.5$ channels, likely in a ROS and CaMKII-dependent manner, although more research is needed to confirm this.

2. Introduction

Breast cancer is the most common cancer in the UK year on year and the most common cancer in women with over 55,000 new cases each year (Łukasiewicz *et al*., 2021). A subset of these, named triple negative breast cancers (TNBCs), is capable of expressing cardiac-type voltage-gated sodium channels (VGSCs) (Brackenbury *et al*., 2008). These channels have been shown to have their activity augmented by the use of doxorubicin in cardiomyocytes (Cappetta *et al*., 2017), although the effects of the drug on these channels in breast cancer cells is not known.

2.1. VGSCs in Cancer

VGSCs are expressed on metastatic cancer cells, such as those in TNBC (Brackenbury *et al*., 2008; Brackenbury., 2012; Mao *et al*., 2019; Angus, Ruben., 2019). The expression of VGSC subtypes varies greatly between cancer types. For example, $Na_v1.5$ is primarily upregulated in breast, colorectal, ovarian and leukemic cancers while $Na_v1.7$ is often upregulated in prostate, lung, stomach and endometrial cancers (Lopez-Charcas *et al*., 2021). VGSCs have been linked to the promotion of proliferation, invasion and metastasis in these cancers (Roger *et al*., 2003; House *et al*., 2010; Nelson *et al*., 2015; Mao *et al*., 2019). The precise mechanisms for how VGSCs exert these pro-tumour features are still unclear, though increases in migration have been proposed to be linked to alterations to the membrane potential of the cancer cells (Yang *et al*., 2020) while increases in invasion and proliferation have been linked to alterations in Na^+ handling (Leslie., 2019). Expression of different VGSC subtypes in cancers is shown in Table 2.1.

Table 2.1 ***VGSC subtype expression in cancer***

Protein	TTX sensitivity	Cancer type
$Na_v1.1$	Sensitive	Ovarian
$Na_v1.2$	Sensitive	Cervical, mesothelioma, ovarian, prostate
$Na_v1.3$	Sensitive	Ovarian, prostate, small cell lung cancer
$Na_v1.4$	Sensitive	Cervical, ovarian, prostate
$Na_v1.5$	Resistant	Breast, colon, lymphoma, neuroblastoma, non-small cell lung cancer, ovarian, small cell lung cancer
$Na_v1.6$	Sensitive	Breast, cervical, lymphoma, melanoma, mesothelioma, non-small cell lung cancer, prostate, small cell lung cancer
$Na_v1.7$	Sensitive	Breast, cervical, lymphoma, mesothelioma, non-small cell lung cancer, ovarian, prostate
$Na_v1.8$	Resistant	-
$Na_v1.9$	Resistant	Lymphoma, small cell lung cancer

2.2. VGSC structure and function

VGSCs are classically found in a range of tissues including neurons, cardiomyocytes and skeletal muscle cells, where they exert their primary role in voltage-induced entry of Na^+ into the depolarising cell, thus initiating or propagating action potentials (Lopez-Charcas *et al.*, 2021). VGSCs are composed of a pore-forming α-subunit and at least one β-subunit, that acts as an adhesion molecule and controls the voltage-dependent gating of the α-subunit (Yu, Catterall., 2003; Brackenbury, Isom., 2008; Gradek *et al.*, 2019). The general structure of a VGSC is shown in Figure 2.1. There are 9 pore-forming α-subunits, $Na_v1.1$-$Na_v1.9$ (encoded by the genes *SCN1A*-*SCN11A*). These are shown in Table 2.1. (Goldin *et al.*, 2000; Brackenbury, Isom., 2008; Xu *et al.*, 2019). These subunits also subtly differ by tissue distribution, albeit with a degree of overlap. $Na_v1.1$, $Na_v1.2$, $Na_v1.3$ and $Na_v1.6$ are generally abundant in the central nervous system (CNS) whilst $Na_v1.7$, $Na_v1.8$ and $Na_v1.9$ are typically more prevalent in the peripheral nervous system (PNS). $Na_v1.4$ and $Na_v1.5$, however, are present in muscle cells, with $Na_v1.4$ being primarily located in skeletal muscle and $Na_v1.5$ in cardiomyocytes (Goldin *et al.*, 2000; Wang *et al.*, 2017; Xu *et al.*, 2019). There are 4 known β-subunits in mammals: β1/β1B, β2, β3 and β4, encoded by the genes *SCN1B*-*SCN4B*, with *SCN1B* being responsible for both β1 and the β1B splice variant, which is developmentally controlled (Brackenbury, Isom., 2011; Hull, Isom., 2017; Bouza, Isom., 2018). These β-subunits belong to the Ig superfamily of cell adhesion molecules (CAMs) as well as playing essential roles in the regulation of the voltage gating of the VGSCs and their cell surface expression (Brackenbury *et al.*, 2008; Brackenbury, Isom., 2011).

The 'gate' of VGSCs lies in the pore domain (PD) between loops 5 and 6 of domain I (Figure 2.1). Within this pore domain, there is also a selectivity filter (SF) which essentially functions to ensure that only Na^+ is able to pass through the channel (Ruiz, Kraus., 2015; Kruger, Isom., 2016; Jiang *et al.*, 2020). This SF is positioned at the narrowest part of the pore in order to distinguish ions with a similar size and charge from other non-specific ions. The SF is always composed of the so-called DEKA ring made up of aspartate (D), glutamate (E), lysine (K) and alanine (A). These residues are positioned in domains I, II, III and IV, respectively (Lukacs *et* al., 2014; Ruiz, Kraus., 2015). Salt bridges such as those between the lysine and glutamate alter the size of the pore, ensuring it is a fit best suited for Na^+ as opposed to other ions of a similar charge such as K^+. Heinemann *et al.* (1992) demonstrated

the importance of this lysine as its replacement abolishes Na^+ specificity completely in VGSCs. In $Na_v1.5$ specifically, the DEKA ring residues have these positions: D371 in domain I, E898 in domain 2, K1419 in domain III and A1711 in domain IV (Ahmed *et al*., 2017).

The pore itself opens in response to a conformational change triggered by the detection of a change in membrane potential (V_m) by the voltage-sensor in loop 4. This conformational change results in the rotation or sliding of loop 4, moving an arginine aside to allow for a gating current to open the pore and allow for ion entry (Vargas *et* al., 2012; Kruger, Isom., 2016). Thus, the 'resting state' of the pore-forming unit in VGSCs is to have the pore blocked as a result of the positioning of loop 4. Further to this voltage-dependent activation mechanism, VGSCs also possess a mechanism of voltage-dependent inactivation. The fast inactivation of these channels is thought to be as a result of the intracellular inactivation loop between domains III and IV (Figure 2.1). This loop is believed to move in such a way as to block the flow of ions through the channel and has been shown to rely on three key residues-isoleucine, phenylalanine and methionine (West *et al*., 1992; Kellenberger *et al*., 1997; Rohl *et al*., 1999). This effective blocking of ion entry is what constitutes fast inactivation of VGSCs. The inactivation gate functions independently of the activation gate and the conformation of the pore of the VGSC, acting as a limiter to determine the maximal depolarisation of the cell in question and prevent the cell from becoming ever more positively charged (Kruger, Isom., 2016).

VGSCs are also targets for a number of selective toxins (Narahashi., 1974), with tetrodotoxin (TTX) being one of the most notable. TTX is often used to essentially sort VGSCs into 2 categories, those that are TTX-sensitive ($Na_v1.1$, 1.2, 1.3, 1.4, 1.6 and 1.7) and those that are TTX-resistant ($Na_v1.5$, 1.8 and 1.9) (Farmer *et al*., 2008; Ruiz, Kraus., 2015). In this case, TTX-resistant Na_v channels are still blocked by TTX, albeit at much higher doses compared to their TTX-sensitive counterparts. A summary of the TTX sensitivity of different VGSCs is shown in Table 2.1.

$Na_v1.5$ is highly expressed in cardiac tissues, compared to other tissue types, and is required for normal cardiac development (Marchal *et al*., 2020). These channels are crucial in the heart for normal function of cardiomyocytes and the control of heart contraction via the regulation of the cardiac action potential. As a result, mutations in these channels, such as in

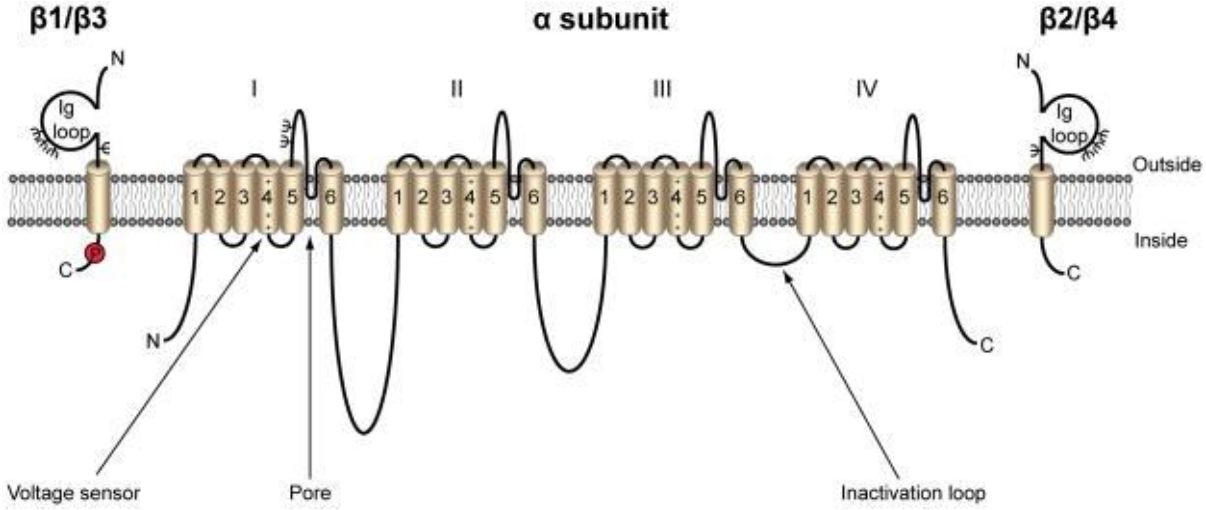

Figure 2.1 ***Basic functional architecture of voltage-gated Na^+ channels (VGSCs).*** *Taken from Brackenbury and Isom., 2008. The pore-forming α-subunit is composed of 4 transmembrane domains, each domain has 6 α-helix segments (S1-6). The pore itself is located between loops 5 and 6 in the first of these domains. S4 in each of the 4 domains is a voltage sensor which, upon activation, leads to a conformational change that moves S4 out of place, allowing for the opening of the pore channel (Wang et al., 2017; Mao et al., 2019). The α-subunit is flanked by 2 β-subunits.*

Table 2.2 ***Genes encoding the 9 key α-subunits of VGSCs along with their primary localisation.***

α-subunit	Gene	Predominant location
$Na_v1.1$	*SCN1A*	Central nervous system
$Na_v1.2$	*SCN2A*	Central nervous system
$Na_v1.3$	*SCN3A*	Central nervous system
$Na_v1.4$	*SCN4A*	Skeletal muscle
$Na_v1.5$	*SCN5A*	Cardiac tissue
$Na_v1.6$	*SCN8A*	Central nervous system
$Na_v1.7$	*SCN9A*	Parasympathetic nervous system
$Na_v1.8$	*SCN10A*	Parasympathetic nervous system
$Na_v1.9$	*SCN11A*	Parasympathetic nervous system

heritable cardiac disorders that lead to the promotion of increased basal activity or changes to the gating kinetics leading to an increase in the persistent Na^+ current, are closely linked to the formation of arrhythmias or diastolic dysfunction (Song, Shou., 2012; Glynn *et al*., 2015).

2.3. Triple Negative Breast Cancer

Breast cancer can be broadly classified into luminal A, luminal B, HER-2 positive and Basal-like (Kennecke *et* al., 2010; Yersal, Barutca., 2014). Luminal A is the most common, making up 50-60% of breast cancer cases. These cancers express oestrogen receptor (oER) and/or progesterone receptor (PR) while being negative for human epidermal growth factor receptor-2 (HER2). These cancers are typically responsive to hormonal therapies or those that block oER or PR function with a 5-year survival rate of 94.4% (Lim, Winer., 2011; Uchida *et al*., 2013; National Cancer Institute., 2018). While there is debate as to whether chemotherapy should be used as standard in addition to these hormonal therapies, there is evidence to suggest that the use of chemotherapeutic drugs such as fluorouracil, epirubicin and cyclophosphamide may give a better disease-free prognosis long term when prescribed in conjunction to hormonal therapies (Uchida *et al*., 2013; Hwang *et al*., 2018). Luminal B cancers are typically more invasive than luminal A tumours, with a worse prognosis overall; these tumours still tend to be oER+/PR+ along with being HER2- but have an enrichment of Ki67, a marker of proliferation (Yersal, Barutca., 2014). Treatment of luminal B cancers can also consist of hormonal therapies due to the likelihood of the cancers being oER/PR+. These cancers are also often treated with aromatase inhibitors such as letrozole, anastrozole and exemestane, with a 5-year survival of 90.7% (Kümler *et al*., 2016; Nabieva, Fasching., 2021). HER2+ breast cancers have an overexpression of HER2 while being negative for both oER and PR (Yin *et al*., 2020; Johnson *et al*., 2020). These tumours make up around 12-20% of breast cancers and are associated with poor prognosis and an aggressive phenotype, with a 5-year survival rate of 84.8%. These cancers are typically treated via the use of one or more chemotherapy drugs in addition to trastuzumab, an anti-HER2 antibody which binds to HER2 and prevents its activation (Slamon *et al*., 2001; Hudis., 2007; Martínez-Sáez, Prat., 2021; Burstein., 2022). The last group, the triple negative (or basal-like) breast cancers (TNBC) accounts for 15-20% of breast cancers and stands out as a point of clinical importance due to its nature as a breast cancer that is especially hard to treat, with a 5-year survival rate of 77.1% (National Cancer Institute., 2018). Due to the lack of oER and PR, these cancers cannot be targeted using hormonal therapies meaning chemotherapeutic drugs must be used.

These typically include taxanes and anthracyclines to target DNA synthesis and repair (Wahba, El-Hadaad., 2015). One such anthracycline is doxorubicin which is currently the most commonly used treatment for TNBC (Denard *et al.*, 2018). Aside from this, novel treatment methods such as poly (ADP-ribose) polymerase (PARP) inhibitors show some promise (Singh *et al*., 2021), though an effective, specific treatment for TNBC is still sorely lacking. This lack of specific treatment for TNBC is paired with TNBCs typically having a highly invasive and metastatic phenotype (Jiao *et al*., 2014; Yin *et al*., 2020). Despite TNBC accounting for up to one fifth of breast cancer cases, an effective and specific therapy targeting TNBCs is much needed considering the high rates of metastasis and rapid mortality for this subtype.

2.4. Membrane potential (V_m)

A V_m arises due to the unequal distribution of charged ions, both positive (such as Na^+ and K^+) and negative (such as Cl^-) inside and outside of the cell, resulting in a difference of voltage across the cell membrane (Yang, Brackenbury., 2013; Cervera *et al*., 2014; Kadir *et al*., 2018). It has been documented that V_m plays crucial roles in terms of both promoting proliferation as well as influencing differentiation in many cell types (Yang, Brackenbury., 2013; Leslie *et al*., 2019). Cells undergoing proliferation tend to have more depolarised cell membranes, whereas terminally differentiated cells have hyperpolarized membrane potentials, and are often quiescent (Kuramoto *et al*., 1981; Sundelacruz *et al*., 2008; Pchelintseva *et al*., 2017; Kadir *et al*., 2018). A similar phenomenon has been observed in cancer, in which tumour cells will have relatively depolarised membrane potentials; -5 to -50 mV in cancer cells versus -50 to -95 mV in their healthy cell counterparts (Yang, Brackenbury., 2013). This depolarised membrane potential results in the promotion of proliferation as well as a more stem-like and less differentiated phenotype as well as generating an increased cancer stem cell pool by encouraging symmetric division of existing CSCs (Yang, Brackenbury., 2013; Leslie *et al*., 2019). Further to this, V_m seems to have links to Ca^{2+} handling via transient receptor potential channels (TRP channels) wherein a more depolarised V_m results in increased intracellular Ca^{2+} via TRP channels (Schwab *et al*., 2012) and, in turn, cytoskeletal organisation (Pettit, Fay., 1998). Due to the importance of Ca^{2+} and 'calcium flickers' at the leading edge in relation to migration of cells, this would seem to propose a link between a more depolarised V_m and increased migratory behaviour in cancer cells (Ridley *et* al., 2003; Wei *et al*., 2012; Yang, Brackenbury., 2013; Tsai *et al*., 2015). In

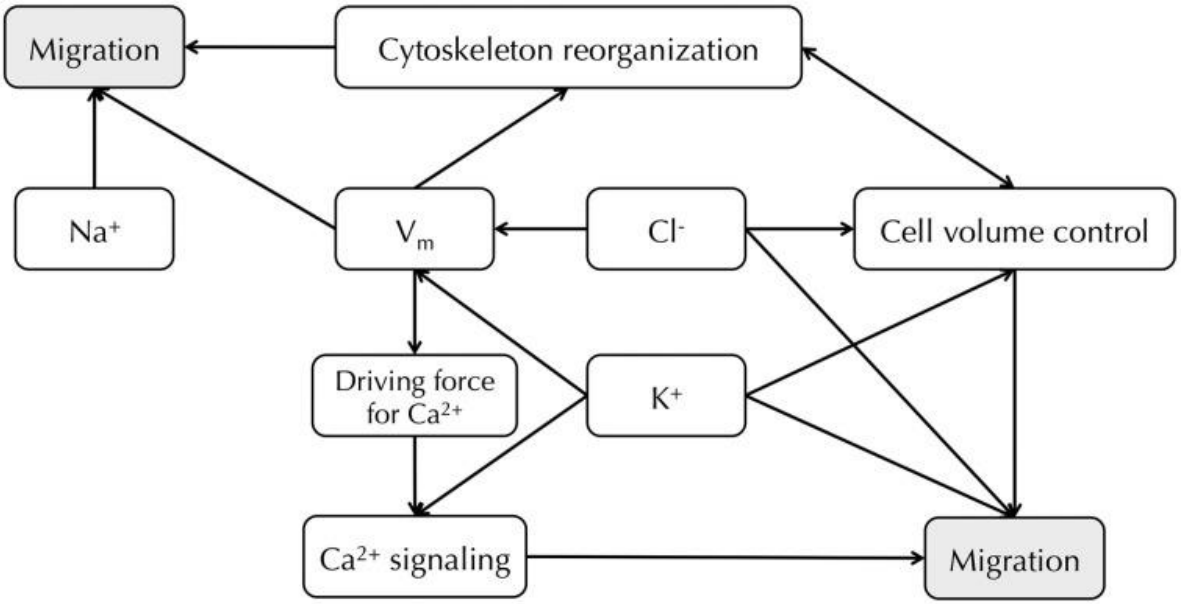

Figure 2.2 ***Relationship between Na^+, K^+, Cl^- channels and Vm in cancer cell migration****, Taken from Yang, Brackenbury., 2013. Changes to membrane potential in cancer cells results in a number of changes to the dynamics and behaviours of the cells including to migration via Ca^{2+} signalling as well as cell volume control and cytoskeletal reorganisation.*

addition to this, the application of electric fields has been demonstrated to increase motility as a result of changes to V_m (Djamgoz *et al*., 2001; Levin., 2003; Schwab *et al*., 2012; Yang, Brackenbury., 2013). A schematic of how V_m fits into the promotion of migration along with changes to intracellular Ca^{2+} and cytoskeletal reorganisation is shown in Figure 2.2.

2.5. Na^+ handling

Linked to this partially depolarised membrane is the existence of a small persistent Na^+current, caused by the steady state incomplete inactivation of VGSCs as a result of the altered membrane potential (Roger *et al*., 2015; Gradek *et al*., 2019). As a result, if the resting membrane potential is constitutively slightly depolarised, there is likely to be a proportion of VGSCs whose activation threshold is below that at which the resting membrane potential sits. The incomplete inactivation of VGSCs leaves a persistent sodium current in place, allowing for the continuous entry of sodium into the cell. This persistent entry of sodium into the cancer cell has been demonstrated to promote proliferation, migration and invasion in tumours where the VGSCs are present (Yang, Brackenbury., 2012; Roger *et al*., 2015; Patel, Brackenbury., 2015; Gradek *et al*., 2019; Leslie *et al*., 2019; Luo *et al*., 2020). The persistent entry of Na^+ results in an increase to the cytosolic Na^+. This has a number of ramifications for Na^+ handling the cells in question; for example, the Na^+/H^+ transporter 1 (NHE1) is responsible for the expulsion of intracellular H^+ in exchange for extracellular Na^+. VGSC-dependent Na^+ influx has been demonstrated to promote NHE1 activity, leading to the efflux of H^+ ions into the extracellular space, lowering the pH of the extracellular environment in caveolae (Brisson *et al*., 2010, Brisson *et al*., 2013), this in turn promotes the activity of cathepsins and the digestion of the extracellular matrix, something that is both essential for invasion of cancer cells and far more effective at a more acidic pH (Busco *et al*., 2010; Brisson *et al*., 2011). While it would be expected that the activity of VGSCs in promoting Na^+ influx would reduce the Na^+ gradient leading to H^+ efflux via NHE1, Brisson *et al* (2013) proposed an allosteric interplay between VGSCs and NHE1. In terms of migration, too, dysregulation of Na^+ handling has significant implications. The Na^+/Ca^{2+} exchanger (NCX) functions typically to import Na^+ and export Ca^{2+} however, in response to increased intracellular Na^+ (or decreased extracellular Na^+), such as via a persistent inward Na^+ current through VGSCs, NCX is capable of operating in reverse mode, expelling Na^+ in exchange for importing Ca^{2+}, resulting in an increase to intracellular Ca^{2+} or, at least a slowing in the extrusion of Ca^{2+}, resulting in the maintenance of higher intracellular Ca^{2+} levels (Tykocki *et*

al., 2012; Zhong *et al*., 2018; Leslie *et al*., 2019). As previously discussed, increases to intracellular Ca^{2+} can in turn have pro-migratory effects on these cells (Ridley *et* al., 2003; Wei *et al*., 2012; Yang, Brackenbury., 2013; Tsai *et al*., 2015). A schematic demonstrating the potential role in changes to Na^{+} handling and intracellular Na^{+} concentration is shown in Figure 2.3.

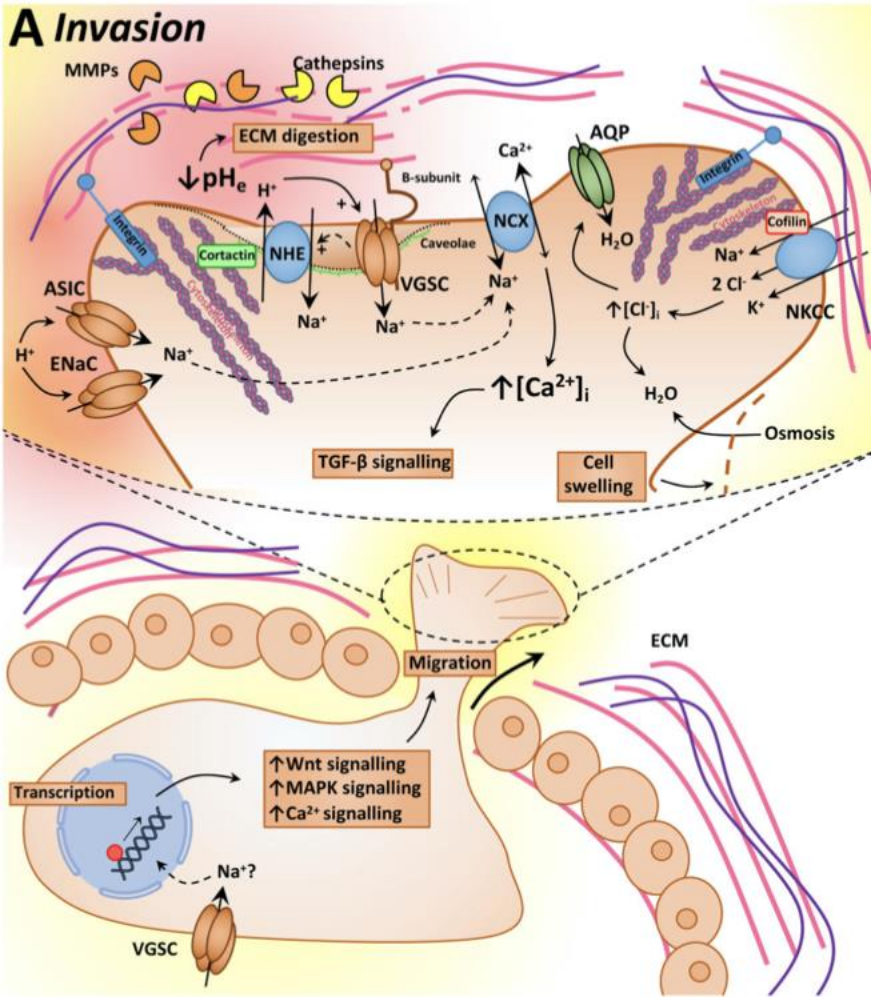

Figure 2.3 ***Effect of elevated Na^+ on cancer progression and the tumour microenvironment.*** *Adapted from Leslie et al., 2019. Increases to intracellular Na^+ as a result of an increased persistent Na^+ current, for example, result in acidification of the extracellular space as a result of NHE activity as well as increased intracellular Ca^{2+} via NCX operating in reverse, promoting cytoskeletal reorganisation and migration. Increased persistent Na^+ current, and intracellular Na^+ also results in increases to Wnt, MAPK and Ca^{2+} signalling, thus altering migration via transcriptional upregulation of these pathways.*

2.6. $Na_v1.5$

A notable example of expression of a VGSC in cancers is the case of $Na_v1.5$ in breast carcinomas. The presence of these VGSCs in breast cancers results in upregulations to migration, proliferation and metastasis (Roger *et al*., 2003; Leslie., 2019). When it comes to the expression of these channels in breast cancers it is not simply an upregulation of functional $Na_v1.5$ channels, rather there exist alternative splice variants of the VGSC. There are two mutually exclusive $Na_v1.5$ splice variants, the 'neonatal' form ($nNa_v1.5$) and the 'adult' form ($aNa_v1.5$) which replaces the $nNa_v1.5$ channels soon after birth (Sarao *et al*., 1991; Gustafson *et al*., 1993; Brackenbury *et al*., 2006). The alternative splicing of Exon 6 results in the use of either the 3' (adult) or 5' (neonatal) exon. This results in 7 amino acid changes in the voltage sensor in domain 1, including the change from a negatively charged aspartate residue (adult) to a positively charged lysine residue (neonatal) (Brackenbury *et al*., 2007; Onkal *et al*., 2008; Fraser *et al*., 2021). This change results in changes to the gating properties and channel kinetics of these VGSCs (Onkal *et al*., 2008; Onkal, Djamgoz., 2009). Despite not typically being expressed long beyond birth anywhere in the body, $nNa_v1.5$ channels have been found to be functionally expressed in breast cancers and breast carcinoma cell lines such as MDA-MB-231, where their expression and activity increase proliferation, invasion and metastasis of these carcinomas (Fraser *et al*., 2005; Nelson *et al*., 2015).

2.7. Doxorubicin - physiological effects

Doxorubicin is an anthracycline drug that is widely used in the treatment of a range of cancers, including TNBC, stomach cancers and leukaemias (Thorn *et al*., 2011; Zhao, Zhang., 2017; Johnson-Arbor, Dubey., 2021). There are two main mechanisms by which doxorubicin is thought to exert its anti-cancer effects. The first mechanism is via the poisoning of Topoisomerase II complexes and the intercalation of the drug itself into the DNA of the target cell. This results in double strand DNA breaks along with changes to chromatin structure leading to the inhibition of DNA synthesis (Yang *et al*., 2013; Agudelo *et al*., 2014; Taymaz-Nikerel *et al*., 2018). At clinical doses, however, the most relevant of these is believed to be the inhibition of Topoisomerase II complexes (Yang *et al*., 2013). The second proposed mechanism of action is based on the formation of reactive oxygen species (ROS) and reactive nitrogen species (RNS) via the metabolism of the drug by a number of enzymes including NADH dehydrogenase, xanthine oxidoreductase and cytochrome p450

reductase (Taymaz-Nikerel *et al*., 2018; Songbo *et al*., 2019; Kalyanaraman., 2020; Prasanna *et al*., 2020). These reduction reactions result in a semiquinone intermediate possessing the ability to rapidly react with and reduce oxygen to produce superoxide anions (O_2^-), resulting in a redox cycle propagated by these superoxide anions reacting with nitric oxide to then produce RNS, exacerbating the oxidative damage (Songbo *et al*., 2019; Kalyanaraman., 2020; Prasanna *et al*., 2020). The knock-on effects of this oxidative damage are far reaching, and one crucial example of this is in altered Ca^{2+} handling (Figure 2.4).

Doxorubicin treatment has been linked to increased intracellular Ca^{2+} and Ca^{2+} release from the sarcoplasmic reticulum (SR) or endoplasmic reticulum (ER) which may contribute to cytosolic Ca^{2+} overload in response to doxorubicin (Cappetta *et al*., 2017; Tscheschner *et al*., 2019; Rawat *et al*., 2021). Doxorubicin is thought to promote Ca^{2+} release from the SR or ER via sensitization of ryanodine receptors (Kim *et al*., 1989), where it was shown that doxorubicin promoted Ca^{2+} release in the same way as caffeine, via a similar interaction. It has been demonstrated, more recently, that doxorubicin binds directly to the cardiac-type ryanodine receptor (RyR2), and in turn stimulates Ca^{2+} release in cardiac cells (Saeki *et al*., 2002). There are three mammalian isoforms of ryanodine receptors named RyR1, RyR2 and RyR3. These isoforms are primarily located in skeletal muscle, cardiac tissue and brain tissue, respectively (Lanner *et al*., 2010). A more recent paper by Abdoul-Azize *et al.* in 2018 suggested that a similar increase in intracellular Ca^{2+} was occurring in the TNBC cell line MDA-MB-231 in response to doxorubicin. However, they propose that this increase is predominantly linked to increased expression of TRP channels. TRP channels make up the store operated Ca^{2+} system (SOC), responsible for the movement of Ca^{2+} into the cell from the extracellular space. This implies that the increase of cytosolic Ca^{2+} is coming from the extracellular space as well as from the intracellular stores, although the mechanism behind the release from intracellular stores is not clear in cancer cells as it is in cardiomyocytes as described above (Abdoul-Azize *et al*., 2018). Another element to consider in the interaction between doxorubicin and intracellular Ca^{2+} is that doxorubicin has been shown to modulate the sarco/endoplasmic reticulum Ca^{2+} ATPase (SERCA), specifically SERCA2, present on the surface of the sarcoplasmic and endoplasmic reticulum. These SERCA pumps play a crucial role in Ca^{2+} reuptake into the intracellular stores and, in response to treatment with doxorubicin, their expression has been reported to be reduced, which would in turn result in a persistent release of Ca^{2+} from the intracellular stores (Arai *et al*., 2000; Zhang *et al*., 2014; Wenningmann *et al*., 2019).

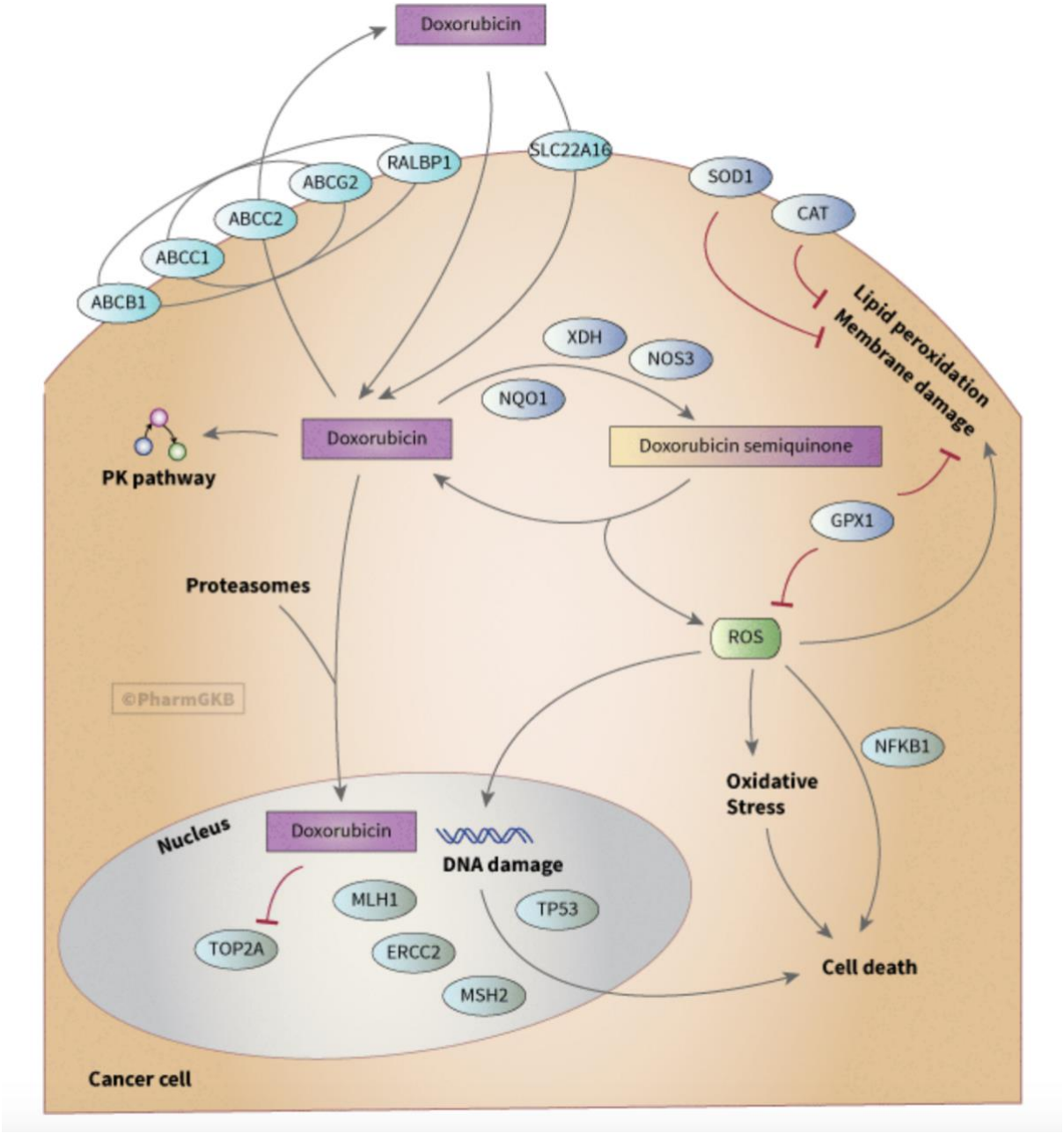

Figure 2.4 ***Intracellular pathways of doxorubicin.*** *Taken from PharmGKB. Doxorubicin promotes production of ROS via its conversion to a semiquinone form via interactions with a number of enzymes. This results in the production of oxygen radicals which result in oxidative stress, DNA damage and eventually the death of the cell. Doxorubicin also enters the nucleus where it poisons topoisomerase II and intercalates itself into the DNA of the cell preventing DNA replication and synthesis. An interactive version of this schematic is available at PharmGKB here: pharmgkb.org/pathway/PA165292163*

2.8. Doxorubicin – effects on $Na_v1.5$

The clinical usage of doxorubicin is hindered by the high incidence of cardiotoxicity, and resultant cardiac dysfunction, associated with higher doses of the drug (Cappetta *et al*., 2017; Zhao, Zhang., 2017; Fernandez-Chas *et al*., 2018; Rawat *et al*., 2021). The precise mechanism remains unclear, but it has been linked to increased expression and activity of $Na_v1.5$ VGSCs, specifically with a resulting increase of the persistent Na^+ current, giving Na^+ overload in the cytosol of cardiomyocytes (Cappetta *et al*., 2017; Zhao, Zhang., 2017; Fernandez-Chas *et al*., 2018). The proposed mechanism behind this increase in persistent Na^+ current is shown in Figure 2.5 (Cappetta *et al.*, 2017).

The importance of the doxorubicin-induced Ca^{2+} release is to increase the activation of Ca^{2+}/calmodulin-dependent kinase II (CaMKII). CaMKII is, in turn, capable of phosphorylating $Na_v1.5$ channels at a number of sites (Wagner *et al*., 2006; Herren *et al*., 2011; Herren *et al*., 2015). The most important of these sites may be Serine 571, which has been shown to be phosphorylated by CaMKII as well as have the capacity to promote an increase in the persistent Na^+ current when phosphorylated, as demonstrated by its replacement with a phosphomimetic glutamic acid (Glynn *et al*., 2015). ROS is another, potentially important player in the mechanism underpinning potential effects of doxorubicin on Na^+ current. It was previously thought that ROS itself was capable of acting on $Na_v1.5$ channels, leading to an increase in persistent Na^+ current (Ward and Giles., 1997; Wang *et al.*, 2002; Song *et al*., 2006) while, at a similar time, increased CaMKII activation was being seen to result in a remarkably similar increase to persistent Na^+ current (Song *et al*., 2006; Wagner *et al*., 2006). The two have since been linked and are thought to be one and the same mechanism causing increased persistent Na^+ current (Wagner *et al*., 2011). The key to this mechanism is that ROS itself is, in fact, capable of sustaining activation of CaMKII, independent of the intracellular Ca^{2+} concentration, something that has since been reported as a cause for cardiac dysfunction (Wagner *et al*., 2011; Erickson., 2014; Zhao *et al*., 2020). Thus, ROS oxidises Cysteine 281 and Methionine 282 in the regulatory domain of CaMKIIα. This oxidation results in an activation profile similar to autophosphorylation of the protein resulting in increased activation and activity (Wagner *et al*., 2011; Erickson., 2014; Wang *et al*., 2021). It is this activation that would then promote the phosphorylation of $Na_v1.5$ channels, resulting in an increase to the persistent Na^+ current. In fact, it has been documented that in cardiac tissues, ROS-activated CaMKII plays a key role in the

potentiation of arrythmias and other cardiac dysfunctions (Wagner *et al.*, 2011; Zhang., 2017; Zhao *et al.*, 2020). It is this mechanism that doxorubicin appears to be acting through, promoting an increase in cytosolic ROS to result in the oxidation of CaMKII, giving the activation of the protein and in turn the phosphorylation of $Na_v1.5$ channels in cardiac tissues (Cappetta *et al.*, 2017). The as yet unanswered question is whether the same mechanism may exist in breast cancer cells expressing $Na_v1.5$. However, it is important to note that ROS production has roles in a number of other potential consequences, some of which may affect the expression or activity of $Na_v1.5$. For example, FOXO1 has been down to downregulate $Na_v1.5$ expression in response to ROS in cardiomyocytes (Mao *et al.*, 2012). In addition to this, evidence has shown that an increase in NAD^+ (and thus a decrease in ROS) results in an increase to Na^+ current through $Na_v1.5$ channels, limiting phosphorylation of $Na_v1.5$ at S1503 (Matasic *et al.*, 2020).

The mechanisms described above potentially explain how doxorubicin may have an influence on Na^+ currents through $Na_v1.5$ channels, as proposed by Cappetta *et al.* in 2017, this is visualised in Figure 2.5. They found that treatment with doxorubicin led to an increase in late Na^+ current in cardiomyocytes, contributing to large increases in cytosolic Na^+ and Ca^{2+} resulting in diastolic dysfunction *in vivo*. It is by this mechanism, combined with topoisomerase II inhibition, that doxorubicin is thought to exert its cardiotoxic effects. The element of this which seems uncertain is whether Ca^{2+} or ROS are the key players in this mechanism, or a combination of the two. While doxorubicin is used to treat metastatic breast cancers, and a number of studies have been done using the highly invasive MDA-MB-231 breast cancer cell line (Lao *et al.*, 2013; Pilco-Ferreto, Calaf., 2016; Lovitt *et al.*, 2018; Marinello *et al.*, 2019), no research has been conducted analysing the effects of doxorubicin on Na^+ currents and VGSCs in this cell line. There is also evidence to suggest that doxorubicin promotes migratory behaviour and metastasis in cancer cells that it is used to treat. Liu *et al* (2019) suggest that treatment of the breast cancer cell lines MCF-7 and BT-474 with doxorubicin at sublethal doses promotes migration and invasion in these cell lines via the Rho/myosin light chain pathway. However, the mechanism by which doxorubicin elicits these effects remains unclear (Liu *et al.*, 2019). Additionally, it has been demonstrated that topoisomerase inhibitors (the same class of drug as doxorubicin) can promote cell motility in a range of cancer cell lines including colorectal and small cell lung cancers (Liu J *et al.*, 2019). The latter of these two papers, interestingly, implicates ROS in this promotion of motility via the JAK2-STAT1 pathway (Liu J *et al.*, 2019). However, it is not known

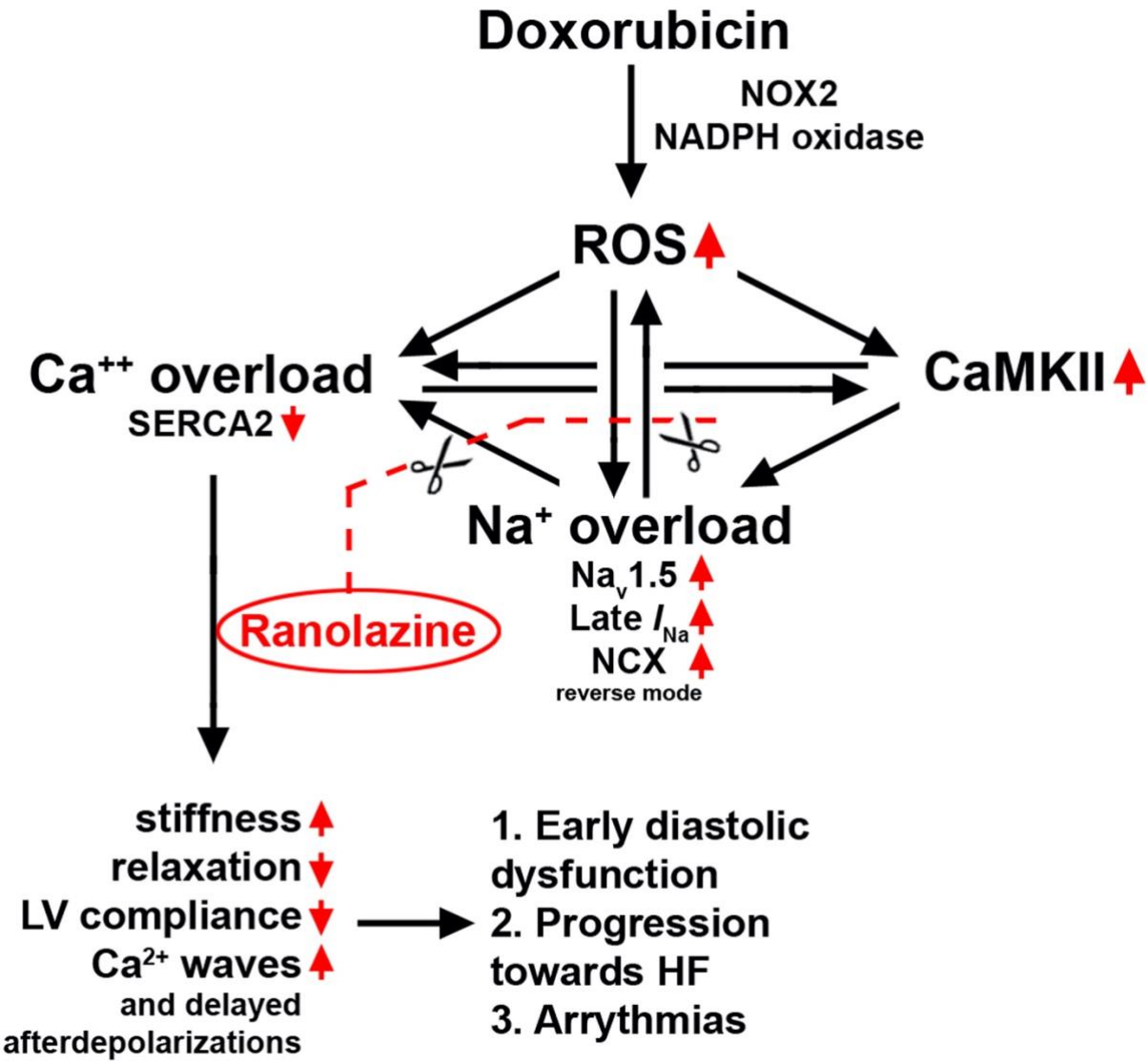

Figure 2.5 ***Schematic illustration of the positive feedback loops leading to Ca^{2+} overload via increased persistent Na^{+} current and consequent cardiotoxicity, induced by doxorubicin.*** *Adapted from Cappetta et al., 2017. Doxorubicin promotes increases to ROS which result in both increases to cytosolic Ca^{2+} contributing to cytosolic Ca^{2+} overload as well as an increase to CaMKII activation via an oxidation reaction. CaMKII is then capable of phosphorylating $Na_v1.5$ resulting in an increased persistent Na^{+} current and, in turn, the increased function of NCX in reverse mode resulting in further increased cytosolic Ca^{2+}. In cardiomyocytes these changes result in diastolic dysfunctions as well as arrhythmias (Cappetta* et al.*, 2017).*

whether doxorubicin has a similar effect on migration or invasion of MDA-MB-231 cells and whether this may be dependent on increased persistent Na^+ current through $Na_v1.5$. Additionally, it is reported that 5 μM approximates to the peak plasma concentration of doxorubicin when used to treat lymphoblastic leukaemia (Hempel *et al.*, 2002). This gives a good starting point for doxorubicin concentration in the experiments.

2.9. Hypothesis and Aims

The overall goal of the experiments described in this thesis was to assess the impact of doxorubicin on the function and activity of $Na_v1.5$ channels expressed in MDA-MB-231 cells. The hypothesis is that doxorubicin has a similar effect on these channels in MDA-MB-231 cells to that reported in cardiomyocytes via either a primarily Ca^{2+} or ROS dependent mechanism, acting through the activation of CaMKII leading to channel phosphorylation and increased persistent Na^+ current. Given that increased Na^+ influx through $Na_v1.5$ channels has been shown to promote an invasive and metastatic phenotype in breast cancer cells (Roger *et al.*, 2003), increased Na^+ current caused by doxorubicin may represent a potential risk of recurrence and metastasis in patients on this treatment. There were three aims:

1. Establish whether treatment with doxorubicin increases persistent Na^+ current in MDA-MB-231 cells.
2. Investigate the mechanism behind any such changes and how this may link to what is reported in cardiomyocytes.
3. Perform a functional output to see how doxorubicin treatment is affecting cell behaviours such as migration or invasion.

3. Materials and Methods

3.1. Cell culture

MDA-MB-231 cells were grown in Dulbecco's Modified Eagle Medium (DMEM) supplemented with 5% foetal calf serum (FCS) and 4 mM L-Glutamine. Cells were grown at 37°C and 5% CO_2 (as described in Nelson *et al.*, 2015). Cells were confirmed to be mycoplasma-free using DAPI imaging (Yang *et al.*, 2012; Nelson *et al.*, 2014).

3.2. Electrophysiology

Whole-cell patch clamp recording was used to measure Na^+ currents from cells seeded onto 13mm glass coverslips (Academy, UK). The cells were recorded in an extracellular physiological saline solution (PSS) containing 144 mM NaCl, 1 mM $MgCl_2$, 5.4 mM KCl, 2.5 mM $CaCl_2$, 5.6 mM D-Glucose and 5 mM HEPES buffer. The PSS was pH tested and altered using 4 M NaOH to give a final pH of 7.2. Prior to recording, growth medium along with any pharmacological treatments was washed off the cells by perfusing with this extracellular solution. Patch pipettes were pulled from glass capillaries (GC150TF-75-Harvard Apparatus, US) using A P97 flaming/frown micropipette puller (Sutter Instruments, US) and tips fire-polished to give resistance of ~8 MΩ when filled with internal solution. The intracellular patch solution contained 5 mM NaCl, 145 mM KCl, 2 mM $MgCl_2$, 1 mM $CaCl_2$, 10 mM HEPES and 11 mM EGTA. The free Ca^{2+} in this pipette solution was calculated to be 24.5 nM (Ca-EGTA Calculator TS v1.3; University of California, Davis; using constants from Schoenmakers' Chelator). This solution was adjusted to pH 7.4 using 1 M CsOH. A Multiclamp 700B amplifier (Molecular Devices, UK) was used to take the voltage clamp recordings, with series resistance compensated for by 40%, in line with recent literature (Leslie *et al.*, 2020). This level of compensation was selected to be safely below the threshold for oscillations in cell recordings. These recordings were digitized using the Digidata 1440A interface (Molecular Devices, UK). Recordings were sampled at 50 kHz and low pass filtered at 10 kHz. Analysis was done using pCLAMP 10.7 software (Molecular Devices, UK). To measure the effect of doxorubicin treatment on transient and persistent Na^+ currents, a repeat depolarisation protocol was used where cells were held at -120 mV for 250 ms before depolarising to -10 mV for 50 ms. This depolarisation was repeated 50 times within each cell recording. To measure the voltage dependence of activation, cells were held at -120 mV for

250 ms before being depolarised to test voltages. These test voltages were in 10 mV increments from -120 to +30 mV. To assess the voltage dependence of steady state inactivation, cells were held at -120 mV for 250 ms followed by pre-pulses in 10 mV steps from -120 to +30 mV for 250 ms before a test pulse to -10 mV for 50 ms (Leslie *et al.* in 2020). Currents were converted to current density by dividing the raw current values by the capacitance of the cell recorded in pF. Electrophysiological recordings from vehicle control and doxorubicin-treated cells were re-collected separately for each experiment. This was done to account for variability in Na^+ current size between cell populations recorded on different dates, as well as avoiding a type 1 statistical error that would have occurred from repeatedly analysing the same vehicle and doxorubicin-only treated datasets.

3.3. Pharmacology

Doxorubicin (Adooq Bioscience, US) was suspended in DMSO to give a stock concentration of 92 mM. This was diluted in PSS for acute perfusion-based application, or in DMEM for pre-treatment of cell cultures. The working concentration in both cases was 5 μM, unless stated otherwise. In the case of pre-treatment, cells were treated with 5 μM doxorubicin in DMEM for 2 hours prior to electrophysiological recordings. Cyclopiazonic Acid (CPA; Merck, Germany) was used in Ca^{2+} imaging experiments to cause Ca^{2+} efflux from the intracellular stores by blocking SERCA2. 5mg was suspended in 1 ml of DMSO to give a stock concentration of 15 mM. The working concentration was 30 μM. KN93 (Cayman, US) was used in both electrophysiological experiments and in ptychographic experiments to block the function of CaMKII, KN93 was dissolved in DMSO to give a stock concentration of 30 mM which was then diluted in either media or PSS to give the working concentration of 5 μM. BAPTA-AM (Abcam, UK) was used in Ca^{2+} imaging and electrophysiological experiments to chelate free intracellular Ca^{2+}. BAPTA-AM was dissolved in DMSO to give a stock concentration of 50 mM which was dissolved in either media or PSS to give the working concentration of 50 μM. Trolox (Calbiochem, Germany) was used for electrophysiological experiments, dissolved in distilled water to give a stock concentration of 40 mM. Due to Trolox being acidic, NaOH was used to adjust to a physiological pH of 7.2. This stock concentration was then diluted in DMEM to give the working concentration of 10 μM. A summary of drugs used, and concentrations are listed in Table 3.1.

*Table 3.1**Drugs used in this project along with their manufacturers and working concentrations***

Drug	Manufacturer	Solvent	Working concentration	Final DMSO % v/v
Doxorubicin	Adooq Bioscience	DMSO	5 μM	0.0054%
KN93	Cayman	DMSO	5 μM	0.01%
BAPTA-AM	abcam	DMSO	50 μM	0.1%
Trolox	Calbiochem	Distilled water	10 μM	N/A
CPA	Merck	DMSO	30 μM	0.2%

3.4. Fura-2 AM fluorescence Ca^{2+} imaging

The ratiometric Ca^{2+} dye Fura-2 AM (PromoKine) was used to measure and monitor cytosolic Ca^{2+}. 5 mg of Fura-2 AM was dissolved in 50µl 20% w/v pluronic F-127 (Sigma) in distilled water and 50µl DMSO to dissolve the Fura-2 AM. MDA-MB-231 cells were seeded onto glass coverslips and loaded with 5 µM Fura-2 in PSS for 40 minutes at room temperature followed by washing with PSS for a further 20 minutes protected from light with agitation before imaging. Cells were imaged using an OLYMPUS BX51WI microscope, 40X water-dipping objective lens (LUMPlanFL), SciCam Pro camera (Scientifica) and controlled by Micro-Manager-2.0 (ImageJ). The dye was excited at 340 nm and 380 nm using a *p*E-340^{fura} (CoolLED) light source. 340 nm and 380 nm wavelength images were taken with 50 ms exposure and 2x2 binning every 5 seconds. Light emitted was at 510 nm for both Ca^{2+} bound and unbound Fura-2. Images were analysed using FIJI (ImageJ, version 2.5.0) to extract fluorescence values at 340 nm and 380 nm. Regions of interest were drawn including a background containing no cells to give background fluorescence to subtract from the cell fluorescence values. A ratio of signal at 340 nm/380 nm was calculated using Excel (Microsoft).

Fura-2 is excited by both 340 nm and 380 nm wavelengths of light dependent on its Ca^{2+} binding status. When free from Ca^{2+}, Fura-2 is excited at 380-nm, whereas when it is bound to Ca^{2+}, this shifts to 340 nm. As a result, data are presented as a ratio of bound (340 nm): unbound (380 nm) Fura-2. As the Fura-2 fluorescence is intracellular, an increase in intracellular Ca^{2+} will result in an increase in the ratio value, hence the units for these experiments are given as Fura-2 ratio of 340 nm/380 nm with 340 being Fura-2 bound to Ca^{2+} and 380 being unbound. For the CPA-based manipulations, cells were recorded in normal PSS for 4 minutes to establish a baseline. CPA in 0 Ca^{2+} buffer containing 1 mM EGTA was perfused onto the cells and maintained for the duration of the CPA response. During this time, the cytosolic Ca^{2+} increased before returning to baseline as the Ca^{2+} was cleared into the extracellular space. The 0 Ca^{2+} buffer is composed of the same as the standard PSS buffer except the $CaCl_2$ is replaced with 1 mM EGTA.

3.5. Amplex red assays

The Amplex red assay was used to measure extracellular reactive oxygen species (ROS) in response to treatment of cells with 0.0054% DMSO (as a vehicle control) or 5 μM doxorubicin. Amplex Red reagent (Invitrogen Molecular Probes) was dissolved in DMSO and used at 50 μM final concentration in cell medium with Horseradish Peroxidase (HRP) (Thermo Scientific) at a final concentration of 0.1 units/ml. Absorbance (OD) at 560 nm was measured using a CLARIOstar micro plate reader (BMG Labtech). All results given from this technique are blank-corrected values, calculated by subtraction of the OD values of blank wells, containing only cell medium along with the Amplex Red mixture, from those containing cells treated with either DMSO or doxorubicin. H_2O_2 was used as a positive control, serially diluted to give a range of concentrations: 50 μM, 25 μM, 12.5 μM, 6.25 μM, 3.175 μM and, as a result, a range of OD values. Cells were cultured to give 60-70% confluency per well. When ready for analysis, growth medium was removed before washing cells once with warmed PBS. Amplex red and HRP mixture was then added with DMSO or doxorubicin. 500 μl total volume was added to each well for a 24-well plate. Absorbance measurements were taken immediately and then at 2-hour intervals up to 6 hours. Between measurements, cells were stored in an incubator at 37ºC and 5% CO_2.

3.6. Ptychography

Cells were seeded into a 24-well plate at a cell density of 8000 cells per well following cell counting. Cells were incubated at 37ºC and 5% CO_2 until ready to be imaged; drugs were added immediately before imaging started. The Livecyte 2 ptychographic imaging system (Phasefocus) was used to image cells treated with 0.00108% DMSO (control), 5 μM doxorubicin or 5 μM doxorubicin + 5 μM KN93. Images were taken from each of 8 wells every 5 minutes over the course of 24 hours to give a time-lapse video. Each field of view was 500 μm x 500 μm. The Cell Analysis Toolbox (Phasefocus) was used for cell tracking and segmentation, resulting in an output file consisting of 1111 tracked variables, defining cells based on the shapes, sizes, textures and dynamics of the treated and untreated cells. CellPhe (Wilson *et al.*, 2021) was then used to compare the values produced from the 1111

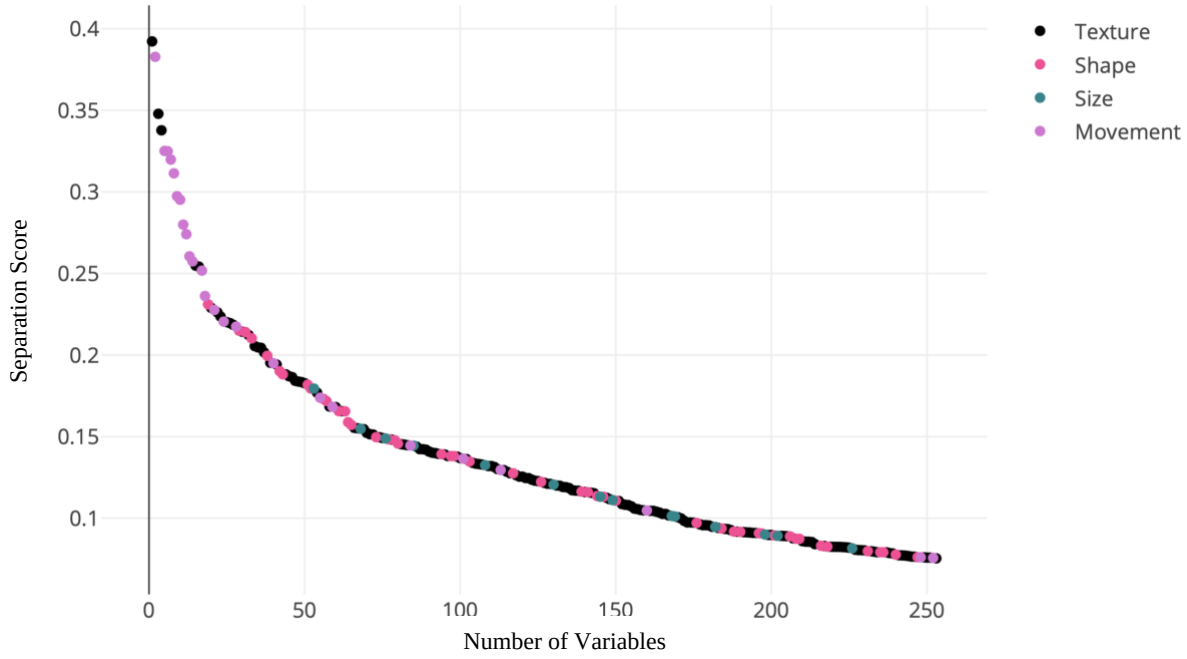

Figure 3.1 ***Separation score analysis of distinguishing variables in treated vs untreated cells.*** *The top 255 variables out of 1111 tracked variables in treated vs untreated cancer cells as imaged with the Livecyte 2 and analysed in CellPhe (Wilson* et al.*, 2021) are shown ranked as well as separated by metric type such as shape and movement. Laura Wiggins assisted with the analysis and production of this figure.*

tracked variables between the treated and untreated conditions, producing separation scores that highlight the variables that show the biggest differences between conditions.

3.7. Data analysis

Data shown are mean and SEM unless stated otherwise. All data analyses were performed using GraphPad Prism (version 9.0.2). Student's t-tests and Mann-Whitney tests were used for 2-sample comparisons between samples dependent on the normality of the data distribution. Normality was determined using Shapiro-Wilk normality tests. For data within samples, paired Wilcoxon tests were used. For the comparison of 3 samples, a one-way ANOVA was used, or a Kruskal-Wallis test followed by a Dunn's post hoc test, if the data was not normally distributed. All statistical tests used are specified in figure legends. Significance was defined as $P < 0.05$. Area under the curve analysis of Ca^{2+} data was performed in Microsoft Excel using the trapezoidal equation $(Y_1 + Y_2) / 2 * (X_2 – X_1)$. A nested t-test was used to evaluate statistical significance of the Ca^{2+} imaging data. Where applicable, 'N' = number of coverslips and 'n' = number of cells. For the CPA manipulations, data were analysed in a nested format to account for variability in cell populations across imaging sessions over separate days. Voltage dependence of activation and inactivation were normalised and fitted to a Boltzmann equation: $G = G_{max}/[1 + \exp((V_{1/2} – V_m)/k)]$ where G is the steady state conductance and G_{max} is the maximum conductance (Leslie *et al*., 2020). Voltage of activation (V_a) was determined using the I/V relationship, the voltage at which current can be first seen is taken as the voltage of activation, this is repeated for each cell recorded. For the ptychography experiments, K means clustering was performed in CellPhe allowing for separation of populations within the doxorubicin-treated group. Cells within groups were also separated using Principal component analysis to show clusters within populations.

4. Results

4.1. 2-hour Pre-treatment with 5 μM doxorubicin increases the persistent, but not transient, Na^+ current

It has been widely reported that prolonged treatment with doxorubicin at high doses results in cardiac dysfunction as a result of increased activity of $Na_v1.5$ channels in cardiomyocytes. Due to the fact that physiological effects of doxorubicin are more pronounced at both higher concentrations as well as over longer periods of time (Lüpertz *et al.*, 2010), the first experiment was to treat the cells for 2 hours prior to electrophysiological recordings with 5 μM of doxorubicin, with the expectation that it would increase the transient and persistent Na^+ currents. Trypan blue cell viability assays were conducted to assess the effects of pre-treatment with 5 μM doxorubicin on MDA-MB-231 cells over the course of 2 hours (Figure 4.1A). 5 μM doxorubicin was found not to significantly affect cell survival after 2 hours (Figure 4.1A). Vehicle control cells were treated with DMSO at an equal v/v as with the 5 μM doxorubicin for the same time period. Raw activation and inactivation data traces for both vehicle and doxorubicin-treated cells are shown in Figure 4.1B. Pre-treatment with 5 μM doxorubicin was found not to affect the transient Na^+ current (n = 13, Mann-Whitney test; Figure 4.1C) but did, however, significantly increase the persistent Na^+ current (n = 10, Mann Whitney test; Figure 4.1D). The current-voltage (I/V) relationship was plotted for these cells and is shown in Figure 4.1E. From the I/V relationship, the voltage of activation (Va) and voltage at peak current (Vp) were measured for each cell. There was no significant effect of 5 μM doxorubicin pretreatment on either parameter (Table 4.1). The activation and inactivation profiles were plotted and are shown in Figure 4.1E and F, respectively. These curves were fitted to Boltzmann functions to obtain the $V_{1/2}$ and slope factor (k) for both activation and inactivation. Again, doxorubicin pre-treatment had no effect on these parameters (Table 4.1). Time to peak (T_p) as well as fast and slow time constants of inactivation (τ_f and τ_s respectively) at 0 mV were also measured. Once again, no significance was seen between conditions. Finally, there was also no effect of doxorubicin pretreatment on the whole cell membrane capacitance (C_m) (Table 4.1).

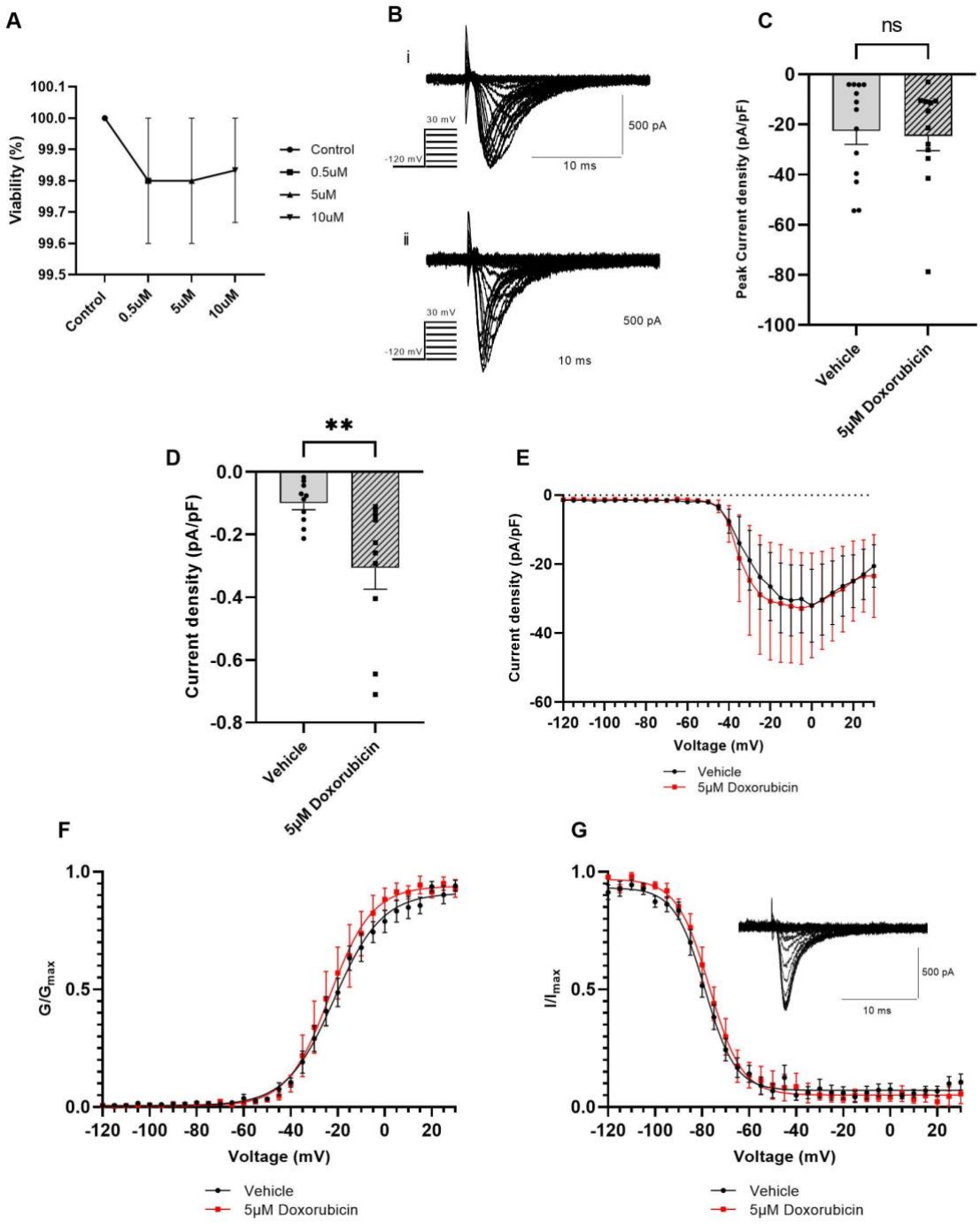

Figure 4.1 ***Electrophysiological analysis of MDA-MB-231 cells pre-treated with 5 μM doxorubicin.*** ***A****- Trypan blue cell viability assay of cells treated with DMSO with a volume/volume equal to that of the highest doxorubicin concentration, 0.5 μM, 5 μM and 10 μM doxorubicin over the course of 2 hours. None of the concentrations tested significantly affected cell viability over the course of 2 hours (n = 3, Kruskal-Wallis test).* ***B****- Representative raw activation traces for vehicle (i) and doxorubicin (ii) treated cells.* ***C****- Analysis of transient Na^+ current, pre-treatment with 5 μM doxorubicin did not significantly affect transient Na^+ current (n = 13, Mann-Whitney test).* ***D****- Analysis of persistent Na^+ current, pre-treatment with 5 μM doxorubicin significantly increased persistent Na^+ current (n = 10, Mann-Whitney test).* ***E****- Current/volage relationship of DMSO vs 5 μM doxorubicin pre-treated cells.* ***F****- Activation curve of DMSO vs 5 μM doxorubicin pre-treated cells.* ***G****- Steady-state inactivation curve of DMSO vs 5 μM doxorubicin pre-treated cells, inset shows a raw steady-state inactivation recording. Data shown as mean ± SEM.*

Parameter	Control	5 μM dox	P-value
V_a (mV)	-48.8 ± 0.82	-49.2 ± 0.83	0.999
V_p (mV)	-1.25 ± 1.57	-1.67 ± 2.11	0.999
C_m (pF)	30.6 ± 2.8	27.6 ± 1.86	0.759
T_p at 0 mV (ms)	1.13 ± 0.09	1.24 ± 0.16	0.776
τ_f at 0 mV (ms)	0.56 ± 0.12	0.52 ± 0.13	0.955
τ_s at 0 mV (ms)	2.36 ± 0.29	2.29 ± 0.27	0.955
Activation, $V_{1/2}$ (mV)	-20.6 ± 3.04	-22.8 ± 4.33	0.680
Activation, *k* (mV)	9.75 ± 1.26	8.89 ± 1.86	0.797
Inactivation, $V_{1/2}$ (mV)	-78.6 ± 1.53	-75.6 ± 3.17	0.352
Inactivation, *k* (mV)	-6.38 ± 0.59	-7.44 ± 1.49	0.864

Table 4.1 ***Pre-treatment with 5 μM doxorubicin did not affect activation or inactivation kinetics.*** *V_a- n = 8, Mann-Whitney test. V_p- n = 8, Mann-Whitney test. C_m- n = 13, Mann-Whitney test. T_p- n = 8, Mann-Whitney test. τ_f- n = 8, Mann-Whitney test. τ_s- n = 8, Mann-Whitney test. $V_{1/2}$ activation- n = 8, Student's t-test. k activation- n = 8, Mann-Whitney test. $V_{1/2}$ inactivation- n = 8, Mann-Whitney test. k inactivation- n = 8, Mann-Whitney test. Data presented as mean ± SEM.*

4.2. Acute application of 5 μM doxorubicin increases transient and persistent Na^+ current in MDA-MB-231 cells

The next experiment conducted to determine the effect of doxorubicin on Nav1.5 Na^+ channels was the direct perfusion of 5 μM doxorubicin while performing a whole-cell patch clamp recording on MDA-MB-231 cells. This allowed for the recording and measurement of both persistent and transient Na^+ currents from a single cell before and after the application of the drug (Figure 4.2). Raw data traces from a representative cell before and after treatment with 5 μM doxorubicin are shown in Figure 4.2A. Analysis of the persistent current alone is shown in Figure 4.2B, between 45 and 50 ms after depolarisation. It was found that the direct application of doxorubicin gave a significant increase to both the transient and persistent Na^+ currents.

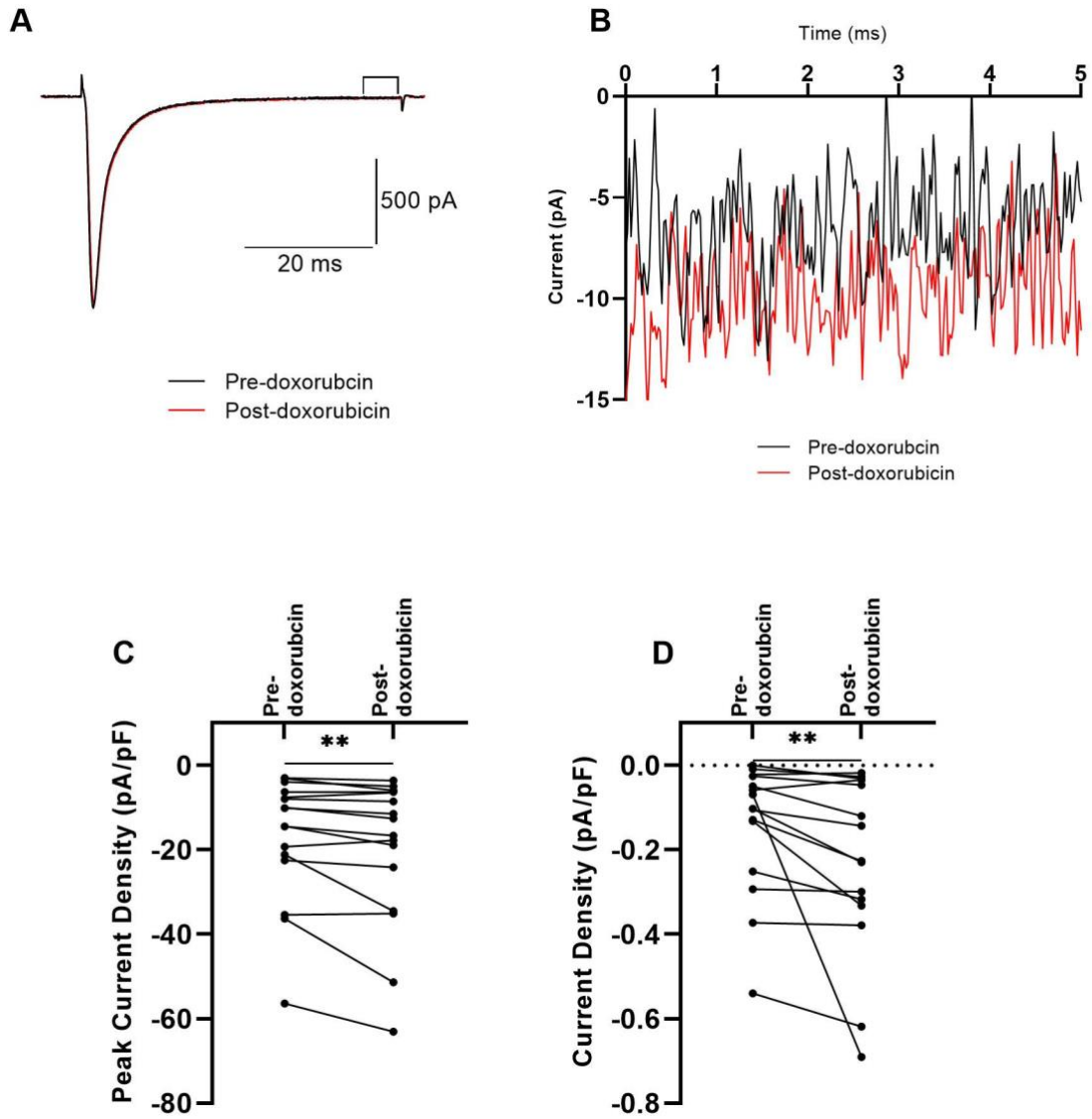

Figure 4.2 ***Direct application of 5 μM doxorubicin increased transient and persistent Na+ current****. **A**- Example raw data traces from Pre- and Post-doxorubicin application overlayed. **B**- Persistent current traces from (A) 45-50 ms after depolarisation. **C**- Transient Na^+ current analysis, treatment with 5 μM doxorubicin significantly increased transient Na^+ current (n = 12, paired Wilcoxon test). **D**- Persistent Na^+ current analysis, treatment with 5 μM doxorubicin significantly increased persistent Na^+ current (n = 12, paired Wilcoxon test).*

4.3. Co-treatment with 5 μM KN93 may prevent increase in persistent Na^+ current in response to 5 μM doxorubicin

Having established that treatment with 5 μM doxorubicin increases the persistent Na^+ current in MDA-MB-231 cells, the next step was to investigate the mechanism behind the increased current elicited by the drug. In cardiomyocytes, CaMKII plays a crucial role in increased persistent Na^+ current and the resultant diastolic dysfunction caused by doxorubicin (Cappetta *et al.*, 2017). Thus, the next experiment was to assess the role of CaMKII in contributing to the increased persistent Na^+ current caused by doxorubicin in MDA-MB-231 cells. To do this, the effect of the CaMKII inhibitor KN93 on blocking the increase in persistent current caused by doxorubicin was investigated (Rokhlin *et al.*, 2010). Due to reports in the literature that co-treatment with KN93 increases the cytotoxicity of doxorubicin (Rodriguez-Mora *et al.*, 2006), guided by the work done in this paper, cell viability assays were performed to select an appropriate concentration of KN93 to use alongside the 5 μM doxorubicin. Trypan blue cell viability assay results are shown in Figure 4.3A using 5 μM KN93, the same concentration used by Rodriguez-Mora *et al.* in 2006. In addition to this, 5 μM KN93 is reported to inhibit CaMKII by around 90% (Sumi *et al.*, 1991). 5 μM KN93 combined with 5 μM doxorubicin did not significantly impact cell viability over 2 hours (Figure 4.3A). Figure 4.3B shows raw whole cell current traces from each of the conditions. Once again, treatment with 5 μM doxorubicin did not affect the transient Na^+ current but increased the persistent Na^+ current (transient- n = 8, Kruskal-Wallis test; persistent- n = 8, Kruskal-Wallis test, Dunn's post-hoc test; Figures 4.3C and D, respectively). This effect on the persistent Na^+ current appeared to be partially recovered by the addition of 5 μM KN93, albeit not significantly, suggesting a potential role for CaMKII in the mechanism. The I/V relationship was not statistically significantly different between conditions (Figure 4.3E). In agreement with this, the V_a and V_p were not significantly different between conditions (Table 4.3). The C_m was also unaffected. Voltage-dependence of activation and steady-state inactivation were also unaffected by doxorubicin and KN93 treatment (Figure 4.3F and G, Table 4.3). Finally, values for T_p as well as both τ_f and τ_s were not significantly different between conditions (Table 4.3).

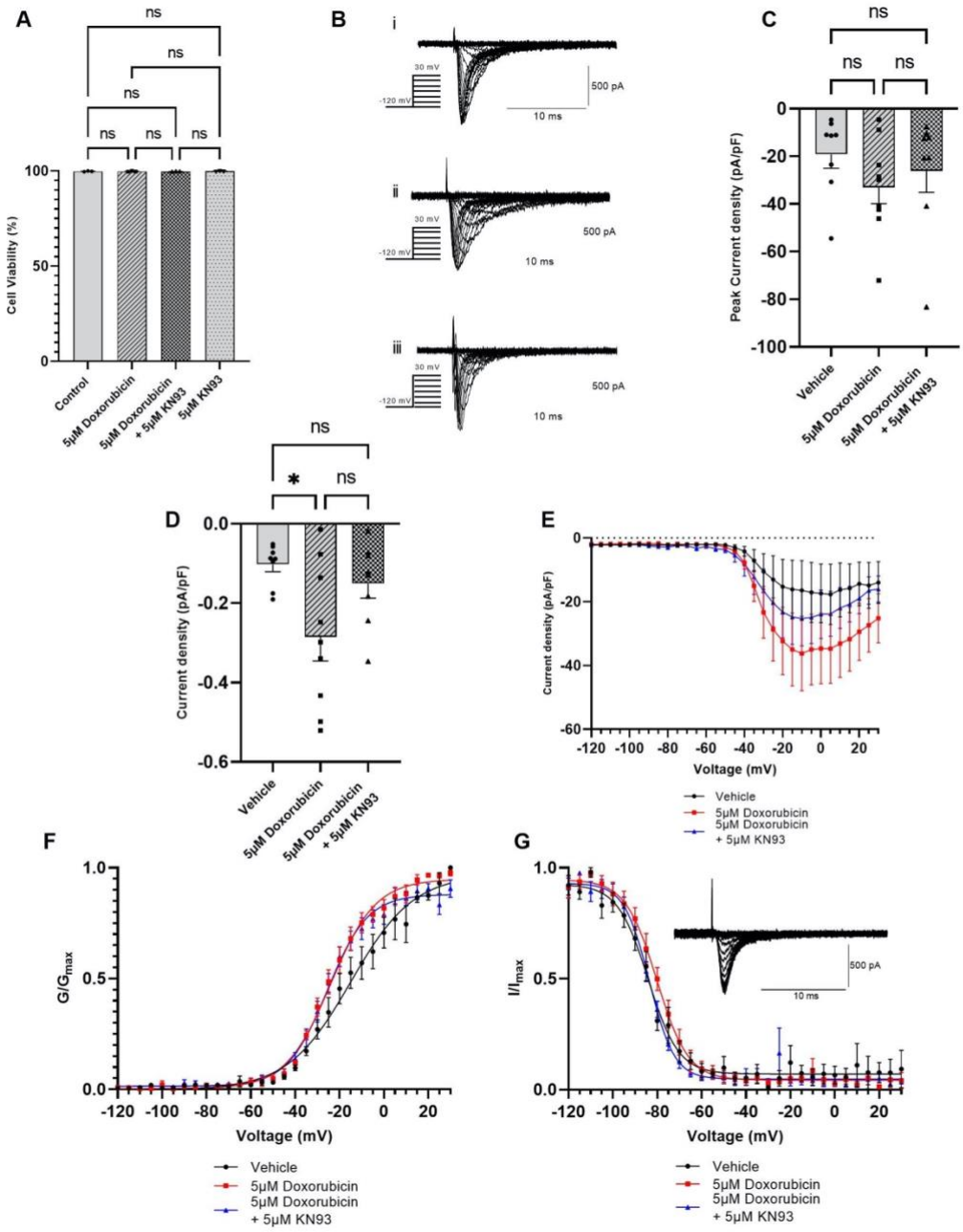

Figure 4.1 ***Electrophysiological analysis of co-treatment of MDA-MB-231 cells with 5 μM doxorubicin and 5 μM KN93***. ***A****- Trypan blue cell viability assay showed treatment with 5 μM doxorubicin, both 5 μM doxorubicin and 5 μM KN93 as well as treatment with 5 μM KN93 alone did not significantly affect cell viability over the course of 2 hours (n = 3, Kruskal-Wallis test).* ***B****- Representative raw activation traces for DMSO treated (i), 5 μM doxorubicin treated (ii) and 5 μM doxorubicin + 5 μM KN93 treated (iii).* ***C****- Analysis of transient Na^+ current, there was no significant difference between conditions (n = 8, Kruskal-Wallis test).* ***D****- Analysis of persistent Na^+ current, treatment with 5 μM doxorubicin significantly increased persistent Na^+ current compared to DMSO vehicle control. Co-treatment with 5 μM KN93 did not significantly mitigate this increase, there was also no significance compared to vehicle control (n = 8, Kruskal-Wallis test, Dunn's post-hoc test.* ***E****- Current/voltage relationships of vehicle vs 5 μM doxorubicin vs 5 μM doxorubicin + 5 μM KN93.* ***F****- Activation curve of vehicle vs 5 μM doxorubicin vs 5 μM doxorubicin + 5 μM KN93.* ***G****- Steady-state inactivation curve of vehicle vs 5 μM doxorubicin vs 5 μM doxorubicin + 5 μM KN93, example raw steady-state inactivation trace shown as an inset. Data presented as mean ± SEM.*

Parameter	Control	5 μM dox	5 μM dox + 5 μM KN93	P-value
V_a (mV)	-50 ± 2.04	-50 ± 1.29	-50.6 ± 1.48	0.955
V_p (mV)	2.50 ± 3.23	0 ± 3.42	1.25 ± 2.46	0.900
C_m (pF)	28.9 ± 3.92	25.0 ± 2.07	23.2 ± 2.21	0.673
T_p at 0 mV (ms)	1.27 ± 0.36	0.92 ± 0.10	1.08 ± 0.12	0.769
τ_f at 0 mV (ms)	0.56 ± 0.33	0.34 ± 0.13	0.31 ± 0.07	0.763
τ_s at 0 mV (ms)	3.04 ± 0.72	2.53 ± 0.52	2.45 ± 0.31	0.603
Activation, $V_{1/2}$ (mV)	-14.9 ± 4.02	-22.3 ± 2.80	-24.4 ± 1.66	0.219
Activation, *k* (mV)	13.7 ± 1.92	10.6 ± 1.63	9.187 ± 0.46	0.276
Inactivation, $V_{1/2}$ (mV)	-85.5 ± 2.57	-80.3 ± 2.16	-83.7 ± 0.87	0.185
Inactivation, *k* (mV)	-7.50 ± 0.91	-6.79 ± 0.71	-5.60 ± 0.36	0.397

Table 4.2 ***Co-treatment with 5 μM doxorubicin and 5 μM KN93 did not affect activation or inactivation kinetics.*** *V_a- n = 4 (vehicle), 7 (5 μM doxorubicin), 8(5 μM doxorubicin + 5 μM KN93), Kruskal-Wallis test. V_p- n = 4 (vehicle), 7 (5 μM doxorubicin), 8(5 μM doxorubicin + 5 μM KN93), Kruskal-Wallis test. C_m- n = 11, Kruskal-Wallis test. T_p- n = 4 (vehicle), 7 (5 μM doxorubicin), 8(5 μM doxorubicin + 5 μM KN93), Kruskal-Wallis test. τ_f- n = 4 (vehicle), 7 (5 μM doxorubicin), 8(5 μM doxorubicin + 5 μM KN93), Kruskal-Wallis test. τ_s- n = 4 (vehicle), 7 (5 μM doxorubicin), 8(5 μM doxorubicin + 5 μM KN93), Kruskal-Wallis test.. $V_{1/2}$ activation- n = 4 (vehicle), 7 (5 μM doxorubicin), 8(5 μM doxorubicin + 5 μM KN93), Kruskal-Wallis test. k activation- n = 4 (vehicle), 7 (5 μM doxorubicin), 8(5 μM doxorubicin + 5 μM KN93), Kruskal-Wallis test. $V_{1/2}$ inactivation- n = 4 (vehicle), 7 (5 μM doxorubicin), 8(5 μM doxorubicin + 5 μM KN93), Kruskal-Wallis test. k inactivation- n = 4 (vehicle), 7 (5 μM doxorubicin), 8(5 μM doxorubicin + 5 μM KN93), Kruskal-Wallis test. Data presented as mean ± SEM.*

4.4. Direct application of 5 μM doxorubicin does not affect cytosolic Ca^{2+}

While the KN93 data does not significantly demonstrate a potential role for CaMKII in the mechanism of doxorubicin-induced increase in persistent Na^+ current, evidence in the literature suggests that it should have an impact: Cappetta *et al.* (2017) show a role for CaMKII in the mechanism increasing $Na_v1.5$ current in cardiomyocytes and KN93 has been shown to be an effective blocker of CaMKII activity (Sumi *et al*. 1991). With this in mind, the next experiment was to investigate the possible role of Ca^{2+} in the process since it is the classical activator of CaMKII. Firstly, 5 μM doxorubicin (or 0.0054% DMSO as a vehicle control) was directly perfused onto cells over the course of 20 minutes and Fura-2 was used to visualise changes in cytosolic Ca^{2+}. A prior study has suggested that the application of doxorubicin results in an increase in cytosolic Ca^{2+} within 3-5 minutes in MDA-MB-231 cells (Abdoul-Azize *et al*., 2018). However, that finding was not replicated here and no measurable increase was observed either from the application of the DMSO vehicle control or 5 μM doxorubicin over the course of 20 minutes (Figure 4.4A and B, respectively). The ionomycin positive control elicited a strong increase in cytosolic Ca^{2+} in both cases.

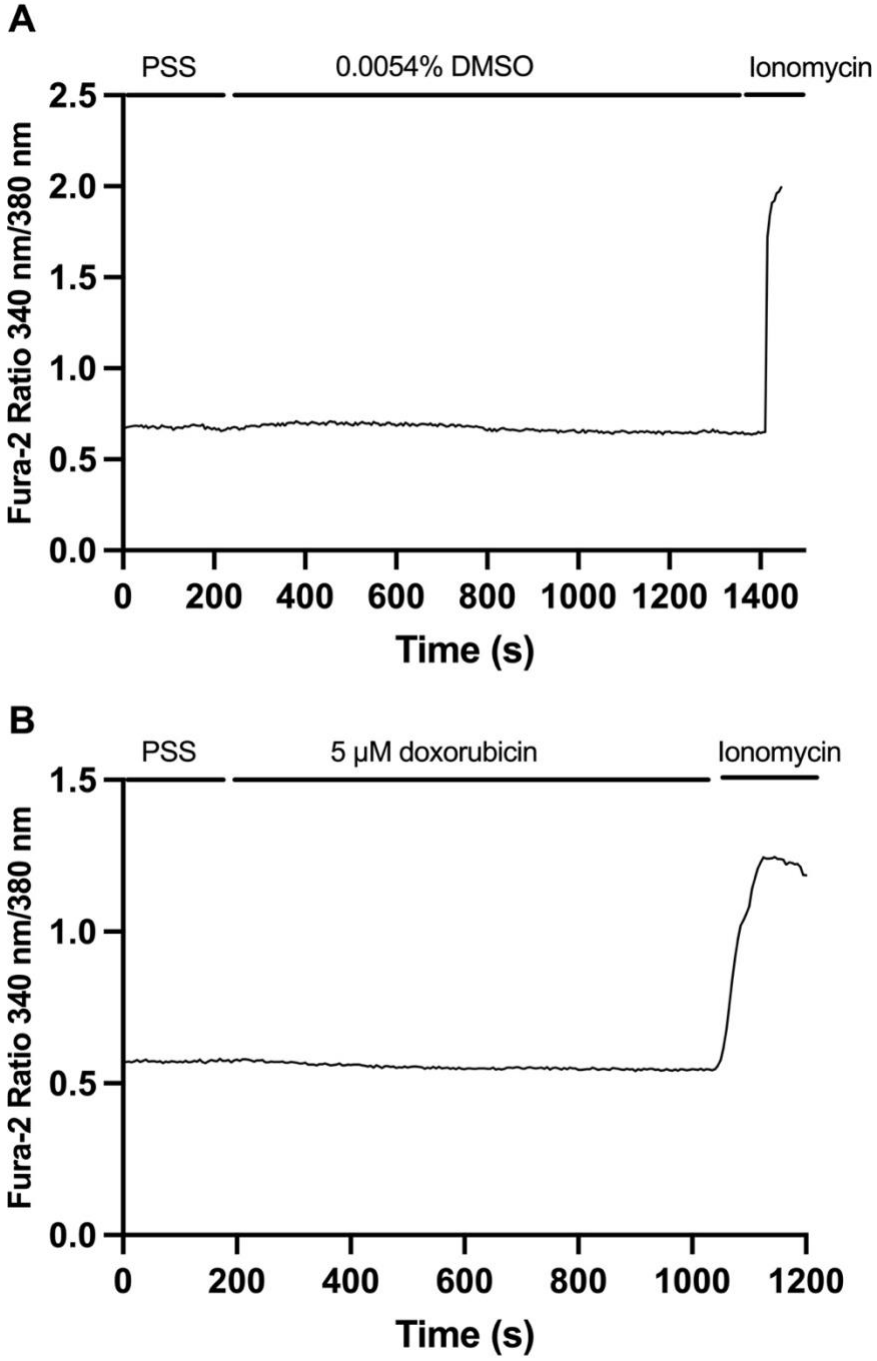

Figure 4.2 ***Direct perfusion of 5 µM doxorubicin does not elicit an increase in cytosolic Ca^{2+}. A****- Representative trace of a recorded cell in response to DMSO application, application of reagents as shown above the trace, ionomycin used as a positive control (n = 3 runs).* ***B****- Representative trace of a recorded cell in response to direct application of 5 µM doxorubicin, application of reagents as shown above the trace, ionomycin used as a positive control (n = 4 runs.*

4.5. Pre-treatment with 5 μM doxorubicin did not affect response to SERCA inhibition by CPA in Ca^{2+} free conditions

After no distinguishable increase in cytosolic Ca^{2+} following the direct perfusion of 5 μM doxorubicin, the next experiment examined whether treatment with doxorubicin affects the intracellular Ca^{2+} stores in the ER. Due to literature detailing potential effects of doxorubicin on SERCA-2 as well as ryanodine receptors (Kim *et al*., 1987; Zhang *et al*., 2014; Wenningmann *et al*., 2019), there was reason to assess whether treatment with doxorubicin is having an impact on intracellular Ca^{2+} stores. CPA in conjunction with 0 Ca^{2+} buffer supplemented with EGTA was used to empty the stores. The 0 Ca^{2+} buffer supplemented with EGTA ensures that the extracellular space is absent of any Ca^{2+}. The rationale behind this experimental strategy is that an interaction between doxorubicin and ryanodine receptors eliciting Ca^{2+} exit from the stores and/or an effect on SERCA-2 inhibiting Ca^{2+} entry to the intracellular stores will result in less Ca^{2+} present in the intracellular stores. Representative traces averaged across 15 cells in one recorded coverslip per condition to give ± SEM for vehicle control (Figure 4.5A) and 5 μM doxorubicin pre-treated cells (Figure 4.5B) are shown. Analysis of both peak fluorescence and the area under the curve revealed no significant difference between conditions, suggesting that treatment with doxorubicin does not result in Ca^{2+} leakage from the intracellular stores (Figure 4.5C and D).

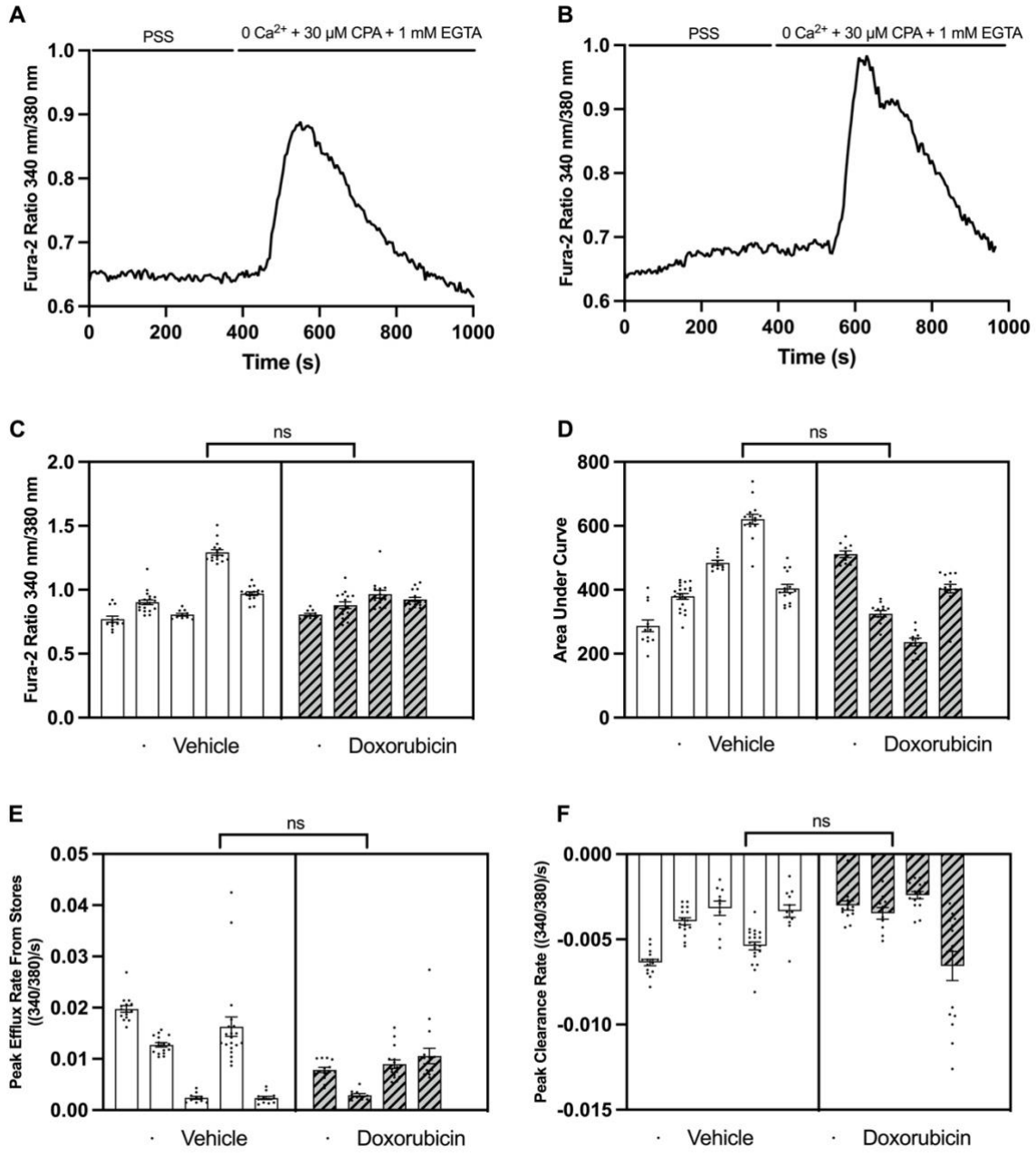

Figure 4.3 ***Pre-treatment with 5 µM doxorubicin does not diminish CPA response***. ***A****- Representative trace of CPA response in cells pre-treated with a DMSO vehicle control. Timings of reagents and their concentrations shown above trace. N = 5, n = 72(vehicle), N = 4, n = 53 (5 µM doxorubicin).* ***B****- Representative trace of a CPA response in cells pre-treated with 5 µM doxorubicin. Concentrations of reagents and the timing of their addition shown above the trace.* ***C****- Nested t-test analysis of the peak fluorescence values for each cell imaged, separated by coverslip (n = 5, 4; Nested t-test).* ***D****- Nested t-test analysis of the area under the curve for each cell imaged, separated by coverslip (n = 5, 4; Nested t-test).* ***E****- Nested t-test analysis of peak efflux rate of Ca^{2+} from the intracellular stores to the cytosol, no significant difference was seen between the vehicle and doxorubicin conditions (n = 5, 4; Nested t-test).* ***F****- Nested t-test analysis of peak clearance rate of Ca^{2+} out of the cytosol to the extracellular space, no significant difference was seen between the vehicle and doxorubicin conditions (n = 5, 4; Nested t-test). Data presented as mean ± SEM.*

4.6. BAPTA-AM suppresses the CPA response in MDA-MB-231 cells

Following the lack of effect of doxorubicin in the Ca^{2+} imaging experiments, BAPTA-AM, an intracellular Ca^{2+} chelator was used to instead evaluate whether blocking Ca^{2+} signalling would suppress the increased persistent Na^{+} current in response to doxorubicin. BAPTA-AM (50 µM) has been used in neurons (Zhang *et al*., 2012) as a strong intracellular chelator with minimal cytotoxicity. Before the use of BAPTA-AM in electrophysiological experiments, a Ca2+ imaging experiment was performed to confirm that 50 µM BAPTA-AM was effective at blocking cytosolic Ca^{2+} increase. Cells were loaded with BAPTA-AM and loaded with Fura-2 before being challenged with CPA. Representative traces of control (Figure 4.6A) and BAPTA-AM treated cells (Figure 4.6B) are shown. These traces demonstrate that the addition of BAPTA-AM suppressed the cytosolic Ca^{2+} rise due to CPA in these cells compared to control.

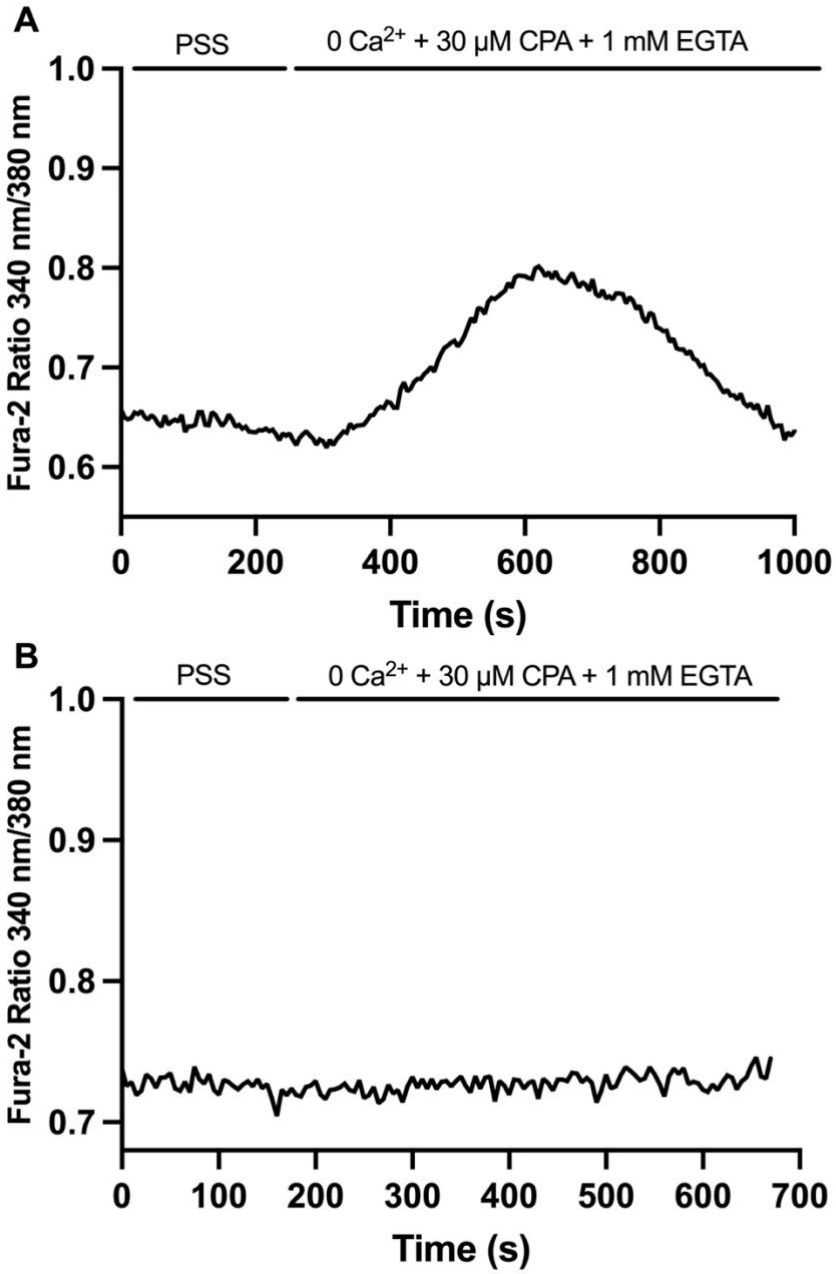

Figure 4.4 ***Pre-loading with 50 µM BAPTA-AM successfully suppresses CPA response***. ***A****- Representative trace of CPA response in cells pre-loaded with a vehicle control of DMSO, reagents, concentrations and time of addition detailed above the trace (n = 2 runs).* ***B****- Representative trace of CPA response in cells pre-loaded with 50 µM BAPTA-AM, reagents, concentrations and times of addition are detailed above the trace (n = 2 runs). Data presented as mean ± SEM.*

4.7. 50 μM BAPTA-AM does not prevent the increase in persistent Na^+ current in response to doxorubicin

Having confirmed that the addition of 50 μM BAPTA-AM successfully suppressed Ca^{2+} release, the effect of BAPTA-AM on the doxorubicin-induced increase in persistent Na^+ current was next investigated using whole cell patch clamp recording. Cells were co-treated with 5 μM doxorubicin and 50 μM BAPTA-AM for 2 hours before recording and compared to doxorubicin alone and vehicle control (Figure 4.7A). As before, treatment with 5 μM doxorubicin resulted in no significant change to the transient Na^+ current (n = 6, Kruskal-Wallis test; Figure 4.7B) but significantly increases the persistent Na^+ current compared to the vehicle control (n = 9, Kruskal-Wallis test, Dunn's post hoc test; Figure 4.7C). Co-application of BAPTA-AM also did not change the transient Na^+ current (Figure 4.7B). In addition, BAPTA-AM had no effect on the increased persistent Na^+ current compared to doxorubicin-only treated cells (Figure 4.7C). The I/V relationships were broadly similar between conditions (Figure 4.7D). C_m, V_a and V_p were unchanged across conditions (Table 4.4). Similarly, there was no significant difference between the three conditions for T_p, τ_f or τ_s (Table 4.4). Activation and inactivation curves are shown in Figure 4.7E and F, respectively. From these, no significant differences in the $V_{1/2}$ or k of activation or steady-state inactivation were observed between any of the conditions (Table 4.3).

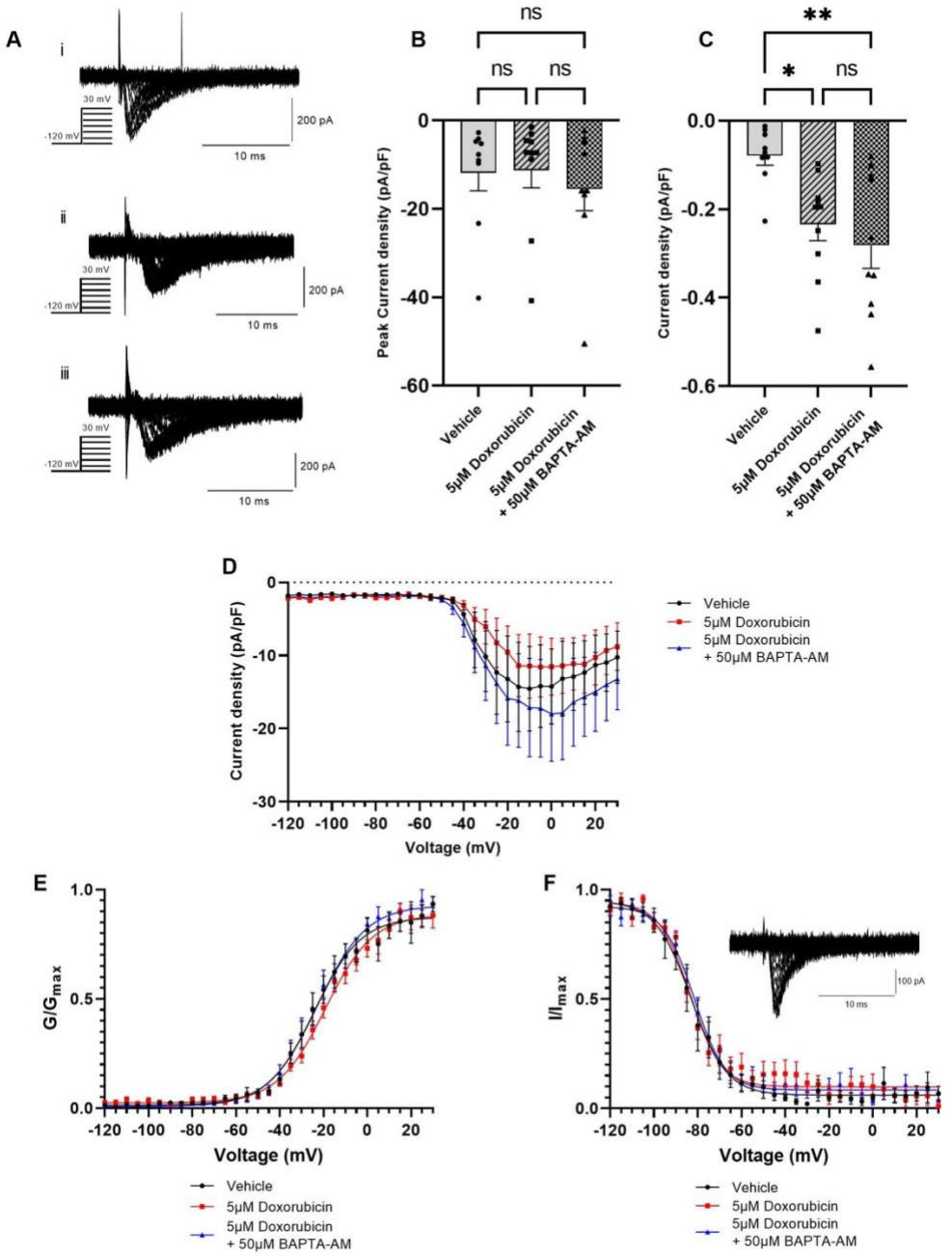

Figure 4.5 **Electrophysiological analysis of co-treatment of MDA-MB-231 cells with 5 μM doxorubicin and 50 μM BAPTA-AM. A**- Representative raw activation traces of vehicle (i), 5 μM doxorubicin (ii) and 5 μM doxorubicin + 50 μM BAPTA-AM (iii) treated cells. **B**- Analysis of transient Na^+ current, there was no significant difference between conditions (n = 9, Kruskal-Wallis test). **C**- Analysis of persistent Na^+ current, treatment with 5 μM doxorubicin gave a significant increase in persistent Na^+ current compared to vehicle, treatment with 5 μM doxorubicin + 50 μM BAPTA-AM also gave a persistent Na^+ current significantly larger than that of the vehicle control. There was no significance between the 5 μM doxorubicin-treated cells and those treated with 5 μM doxorubicin + 50 μM BAPTA-AM (n = 9, Kruskal-Wallis test, Dunns post hoc test. **D**- Current/voltage relationship of vehicle, 5 μM doxorubicin and 5 μM doxorubicin + 50 μM BAPTA treated cells. **E**- Activation curve of vehicle, 5 μM doxorubicin and 5 μM doxorubicin + 50 μM BAPTA treated cells. **F**- Steady-state inactivation curve of vehicle, 5 μM doxorubicin and 5 μM doxorubicin + 50 μM BAPTA treated cells, example raw trace of steady state inactivation shown as an inset. Data presented as mean ± SEM.

Parameter	Control	5 μM dox	5 μM dox + 50 μM BAPTA-AM	P-value
V_a (mV)	-49.2 ± 0.83	-49.4 ± 1.13	-49.3 ± 0.71	0.995
V_p (mV)	0 ± 3.65	0.63 ± 1.752	0.71 ± 2.02	0.987
C_m (pF)	23.0 ± 0.84	22.6 ± 1.40	20.4 ± 1.21	0.305
T_p at 0 mV (ms)	1.13 ± 0.09	1.04 ± 0.11	1.03 ± 0.11	0.591
τ_f at 0 mV (ms)	0.42 ± 0.17	0.43 ± 0.14	0.43 ± 0.14	0.957
τ_s at 0 mV (ms)	1.97 ± 0.30	2.56 ± 0.52	2.24 ± 0.31	0.895
Activation, $V_{1/2}$ (mV)	-23.6 ± 2.20	-21.1 ± 1.27	-22.9 ± 3.53	0.419
Activation, *k* (mV)	9.86 ± 1.17	10.9 ± 0.92	10.2 ± 1.04	0.851
Inactivation, $V_{1/2}$ (mV)	-83.1 ± 4.38	-82.4 ± 1.49	-82.1 ± 2.24	0.846
Inactivation, *k* (mV)	-5.99 ± 0.51	-7.84 ± 1.62	-6.89 ± 1.33	0.622

Table 4.3 ***Co-treatment with 5 μM doxorubicin and 50 μM BAPTA-AM did not affect activation or inactivation kinetics****. V_a- n = 9, Kruskal-Wallis test. V_p- n = 9, Kruskal-Wallis test. C_m- n = 9, Kruskal-Wallis test. T_p- n = 9, Kruskal-Wallis test. τ_f- n = 9, Kruskal-Wallis test. τ_s- n = 9, Kruskal-Wallis test. $V_{1/2}$ activation- n = 9, One-way ANOVA. k activation- n = 9, Kruskal-Wallis test. $V_{1/2}$ inactivation- n = 9, Kruskal-Wallis test. k inactivation- n = 9, Kruskal-Wallis test. Data presented as mean ± SEM.*

4.8. Addition of 5 μM doxorubicin increases extracellular ROS over the course of 6 hours

With previous experiments suggesting that Ca^{2+} may not be important in the mechanism underpinning the increased persistent Na^{+} current in response to doxorubicin in MDA-MB-231 cells, the focus moved to ROS. Evidence in the literature suggests that ROS have the potential to sustain and potentiate CaMKII activation, in the absence of Ca^{2+}, via oxidation of key residues to mimic autophosphorylation (Erickson *et al*., 2008, Wagner *et al*., 2012). In order to evaluate whether treatment with doxorubicin was resulting in an increase in ROS, Amplex red assays were performed to measure extracellular ROS over a period of 6 hours following treatment, measuring the optical density (OD) at 2-hour intervals (Figure 4.8). Values were taken from untreated, DMSO vehicle control-treated and 5 μM doxorubicin-treated cells and compared across the three conditions. Notably, there was a significantly higher OD for the 5 μM doxorubicin-treated cells compared to the DMSO-treated and untreated cells, indicating a significant increase in extracellular ROS. The increase in OD for the cells treated with 5 μM doxorubicin suggests that doxorubicin is promoting ROS production during the 6-hour time course, compared to both the control and DMSO-treated cells.

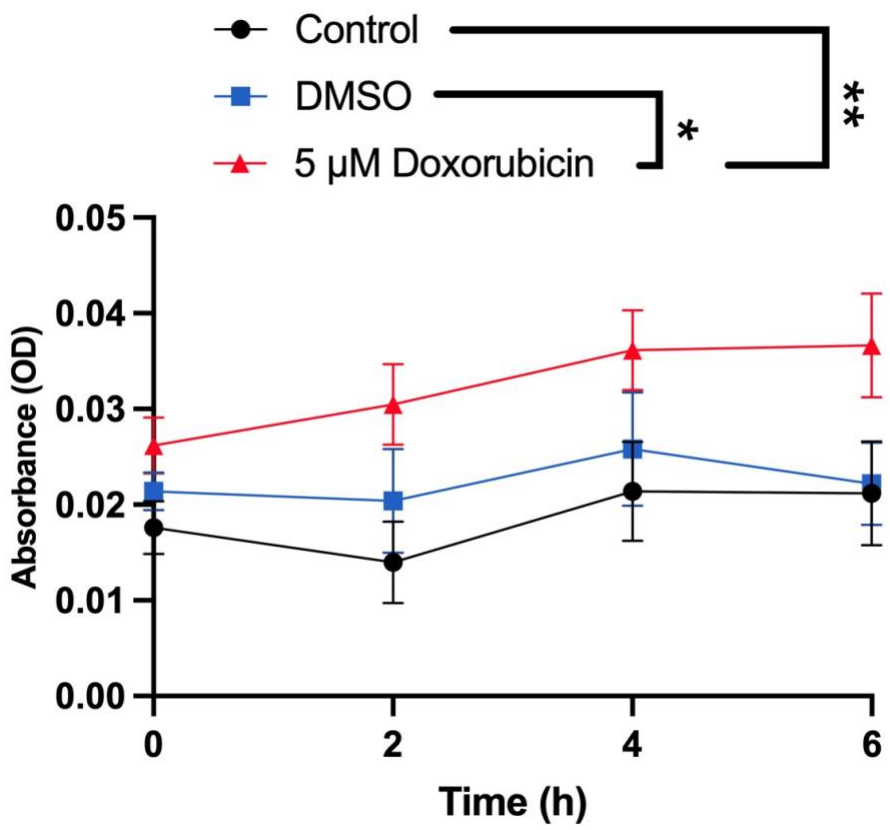

Figure 4.6 Amplex red assay analysis of extracellular ROS in response to DMSO vehicle control and 5 µM doxorubicin. *Time course experiment measuring ROS over 6 hours. Recordings taken at 0, 2, 4 and 6 hours after DMSO or doxorubicin application. Control is medium in the absence of either DMSO or doxorubicin. Data analysed using a one-way ANOVA with a Tukey post-hoc test. The doxorubicin condition showed a significantly higher OD compared to both the control and the DMSO treated cells. Data presented as mean ± SEM. Theo Issitt assisted with the use of the Clariostar plate reader and preparation of the Amplex Red mixture.*

4.9. Co-treatment with 10 μM Trolox may mitigate increase in persistent Na^+ current in response to doxorubicin

Having established the presence of increased ROS in response to addition of 5 μM doxorubicin, the next experiment tested whether ROS were involved in the mechanism underlying the doxorubicin-induced increase in persistent Na^+ current. An intracellular antioxidant, Trolox, was used to mitigate excess ROS in response to doxorubicin. Trolox is a water-soluble vitamin E derivative, used as a standard in the Trolox Equivalent Antioxidant Capacity (TEAC) assay (van den Berg *et al.*, 1999) as well as having prior usage in MDA-MB-231 cells (Marinello *et al.*, 2015). Cells were pre-treated for 2 hours with 5 μM doxorubicin ± 10 μM Trolox prior to whole-cell patch clamp recording to measure the effects on Na^+ current (Figure 4.9A). As with the previous electrophysiological experiments, there was no significant change to the transient Na^+ current across conditions (n = 8, One-way ANOVA; Figure 4.9B). As before, doxorubicin increased the persistent Na^+ current however, in this set of experiments, the difference was below the level of significance (Figure 4.9C). Co-application of 10 μM Trolox appeared to slightly reduce the persistent Na^+ current compared to 5 μM doxorubicin alone, however, the difference was not statistically significant. The I/V relationships were broadly similar across conditions (Figure 4.9D). In addition, V_a, V_p and C_m values were unchanged (Table 4.4). Activation and inactivation curves are shown in Figure 4.9E and F, respectively. From these, there were no significant differences in the $V_{1/2}$ or k of activation or steady-state inactivation (Table 4.4) across any of the conditions. Finally, the T_p, τ_f and τ_s also showed no significant difference across the three conditions (Table 4.4).

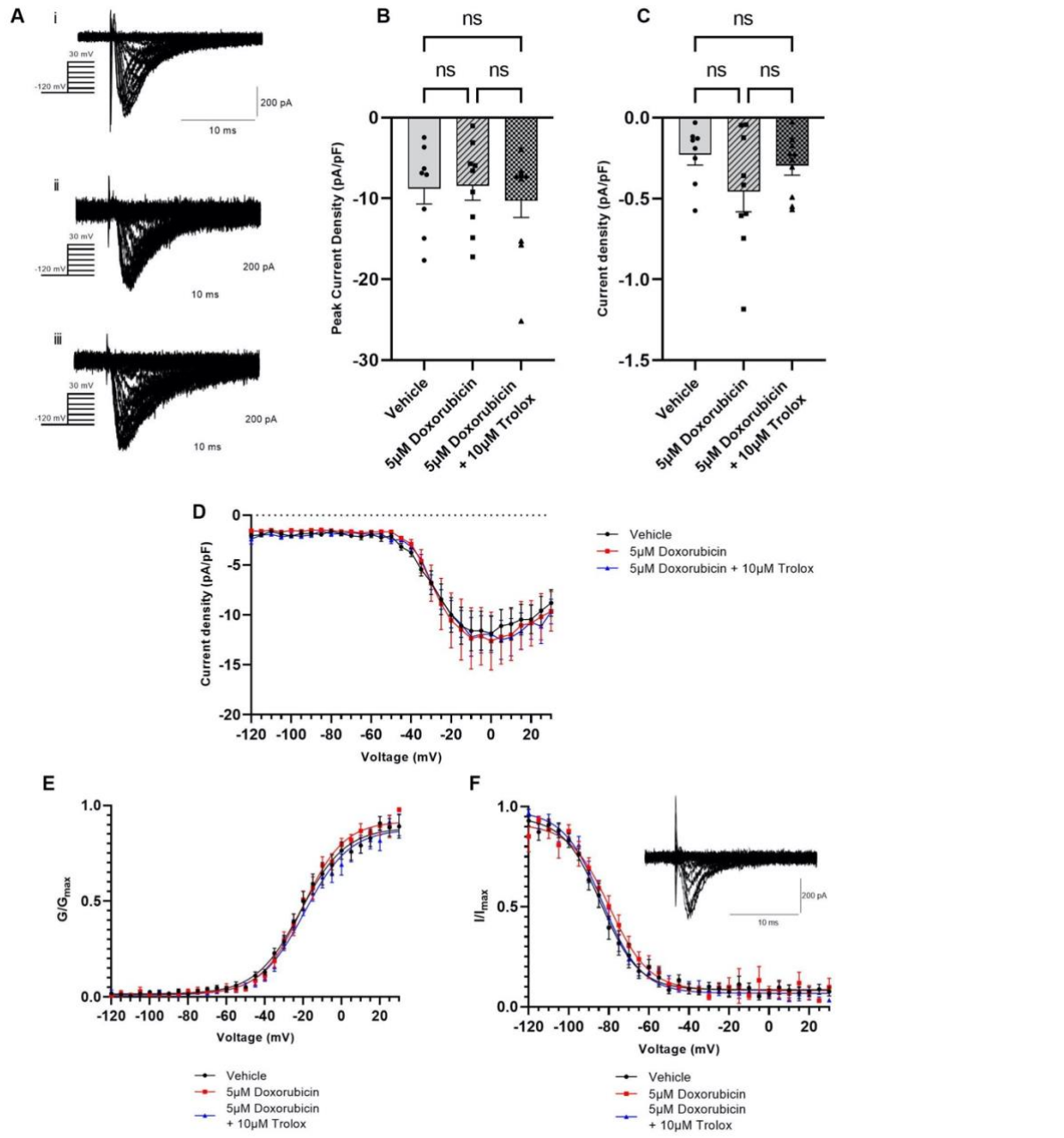

Figure 4.7 ***Electrophysiological analysis of co-treatment of MDA-MB-231 cells with 5 μM doxorubicin and 10 μM Trolox****. **A**- Representative raw activation traces of DMSO vehicle control (i), 5 μM doxorubicin (ii), 5 μM doxorubicin + 10 μM Trolox (iii). **B**- analysis of transient Na^+ current, treatment with 5 μM doxorubicin and/or 10 μM Trolox did not significantly affect transient Na^+ currents (n = 8, One-way ANOVA). **C**- Analysis of persistent Na^+ current, treatment with 5 μM doxorubicin and/or 10 μM Trolox did not significantly affect persistent Na^+ current (n = 8, One-way ANOVA). **D**- Current/voltage relationship for DMSO vehicle, 5 μM doxorubicin and 5 μM doxorubicin + 10 μM Trolox. **E**- Activation curve for DMSO vehicle, 5 μM doxorubicin and 5 μM doxorubicin + 10 μM Trolox. **F**- Steady-state inactivation curve for DMSO vehicle, 5 μM doxorubicin and 5 μM doxorubicin + 10 μM Trolox, example raw steady-state inactivation trace is shown as an inset. Data presented as mean ± SEM.*

Parameter	Control	5 μM dox	5 μM dox + 10 μM Trolox	P-value
V_a (mV)	-50 ± 0.94	-48.6 ± 0.92	-50.7 ± 0.71	0.240
V_p (mV)	0.63 ± 3.05	0 ± 2.89	0.71 ± 1.30	0.979
C_m (pF)	20.8 ± 1.08	23.6 ± 1.12	21.3 ± 1.50	0.637
T_p at 0 mV (ms)	1.19 ± 0.13	1.09 ± 0.11	1.10 ± 0.06	0.748
τ_f at 0 mV (ms)	0.66 ± 0.15	0.65 ± 0.15	0.58 ± 0.09	0.895
τ_s at 0 mV (ms)	2.63 ± 0.40	3.31 ± 0.67	2.74 ± 0.47	0.772
Activation, $V_{1/2}$ (mV)	-20.3 ± 1.93	-19.9 ± 2.72	-18.7 ± 1.87	0.856
Activation, *k* (mV)	10.7 ± 0.88	10.3 ± 0.93	11.1 ± 1.22	0.150
Inactivation, $V_{1/2}$ (mV)	-82.5 ± 2.77	-78.8 ± 3.11	-84.3 ± 2.34	0.386
Inactivation, *k* (mV)	-8.11 ± 1.08	-9.25 ± 1.24	-10.1 ± 1.47	0.396

Table 4.4 ***Co-treatment with 5 μM doxorubicin and 10 μM Trolox did not affect activation or inactivation kinetics.*** *V_a- n = 8, Kruskal-Wallis test. V_p- n = 8, One-way ANOVA. C_m- n = 10, One-way ANOVA. T_p- n = 8, One-way ANOVA. τ_f- n n = 8, One-way ANOVA. τ_s- n = 8, Kruskal-Wallis test. $V_{1/2}$ activation- n = 8, One-way ANOVA. k activation- n = 8, One-way ANOVA. $V_{1/2}$ inactivation- n = 8, One-way ANOVA. k inactivation- n = 8, Kruskal-Wallis test. Data presented as mean ± SEM.*

4.10. Doxorubicin treatment inhibits cell motility *in vitro*

In the final set of experiments, live cell ptychographic imaging was used to measure changes in migration of cells treated with DMSO vehicle control, 5 μM doxorubicin or 5 μM doxorubicin + 5 μM KN93. Cells were imaged every 6 minutes and tracked over the course of 24 hours using LiveCyte imaging software. The raw data was then analysed using CellPhe (Wilson *et al*., 2021). This app allowed for comparison of 1111 variables pertaining to texture, size and dynamics of the cells between treated and untreated conditions as well as ordering of these variables based on separation scores. The 1111 variables were narrowed down to around 250 of the most relevant variables with the highest separation scores between conditions. Images of the cells at the end of the 24 hour treatment period are shown in Figure 4.10A. Within the population of cells treated with 5 μM doxorubicin, K means clustering was performed in CellPhe allowing for separation of populations within the doxorubicin-treated group. This analysis showed that there were two distinct subsets, separated on Principal Component 1 (PC1) (Figure 4.10B), which consists of motility-related variables including the mean velocity of the cells. The mean velocity of cells in each condition was compared in Figure 4.10C. This showed that there was a statistically significant decrease in mean velocity of doxorubicin-treated cells versus vehicle control cells. Furthermore, co-treatment with KN93 did not rescue this defect (Figure 4.10C). However, when the clusters within the doxorubicin-only treated condition are taken into account, compared to the vehicle control, Cluster 1 is comparable to the control cells, as well as having significantly higher mean velocity compared to Cluster 2 (Figure 4.10D). Thus, these data suggest that there is a subpopulation of doxorubicin-treated cells which appear to be resistant to treatment and behave like untreated cells. Further work is required to establish whether CaMKII-mediated increase in persistent Na^+ current predominates in this treatment-resistant, motile population, or whether pharmacological VGSC inhibition blocks the effect.

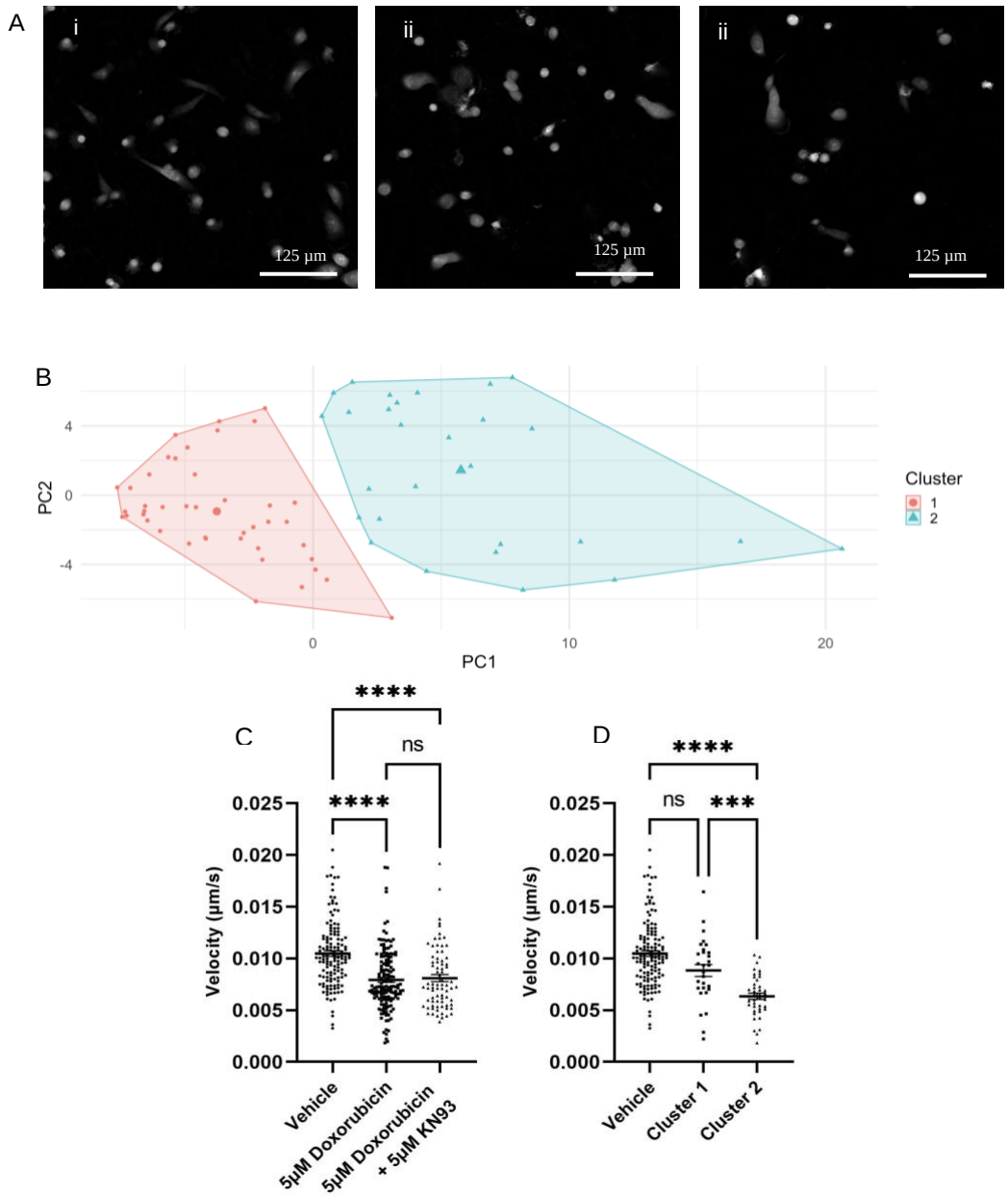

Figure 4.8 ***Live imaging of cells treated with DMSO vehicle control, 5 µM doxorubicin or a combination of 5 µM doxorubicin and 5 µM KN93***. ***A***- *Images of the final frame of the 24-hour ptychographic imaging period for Vehicle control (i), 5 µM doxorubicin (ii) and 5 µM doxorubicin + 5 µM KN93 (iii).* ***B***- *Scatter plot demonstrating clusters withing the 5 µM doxorubicin-treated cells. Cells are separated based on Principle Component (PC) 1, which is made up of motility-related variables.* ***C***- *Whole population analysis of mean velocity of imaged cells. Treatment with 5 µM doxorubicin and 5 µM doxorubicin + KN93 resulted in an overall reduction in velocity of treated cells vs vehicle (Kruskal-Wallis test, n = 138 (vehicle), 144 (5 µM doxorubicin), 77 (5 µM doxorubicin + 5 µM KN93.* ***D***- *Comparison of velocity distinct 5 µM doxorubicin-treated clusters vs vehicle, Cluster 1 is comparable to control while Cluster 2 has significantly reduced velocity compared to vehicle (Kruskal-Wallis test, n = 138 (vehicle), 30 (Cluster 1), 42 (Cluster 2). Data presented as mean ± SEM. Laura Wiggins assisted with the production of the PCA cluster plot and analysis on the CellPhe app.*

5. Discussion

The aim of this research was to examine the effects of doxorubicin treatment on $Na_v1.5$ voltage-gated Na^+ channels in MDA-MB-231 breast carcinoma cells and, should any effects be observed, attempt to elucidate the mechanism behind them. The hypothesis was that treatment with doxorubicin would result in an increase in persistent Na^+ current, similar to that observed in cardiomyocytes (Cappetta *et al.*, 2017). With regards to the mechanism underpinning this anticipated change, the hypothesis was that the mechanism would be Ca^{2+} and CaMKII-dependent with increased CaMKII activation as a result of increased cytosolic Ca^{2+} leading to the phosphorylation of $Na_v1.5$ channels at a number of sites giving an increase to persistent Na^+ current (Wagner *et al.*, 2011; Erickson., 2014; Cappetta *et al.*, 2017). The results of this study support the hypothesis that treatment with doxorubicin increases the persistent Na^+ current, as seen consistently in Figures 4.2, 4.3 and 4.7. The hypothesis regarding the mechanism behind this, however, has not been entirely supported by the results. The CaMKII inhibitor KN93 had a mitigating effect on the increased Na^+ current in response to doxorubicin treatment, albeit not to the point of statistical significance. This may suggest that there is another mechanism involved in the observed effects of doxorubicin on Na^+ current. Further to this, Fura-2 imaging (Figures 4.4 and 4.5) and electrophysiology (Figure 4.7) using the intracellular chelator BAPTA-AM suggest that Ca^{2+} (or at least its sustained presence), is not required for the increased persistent Na^+ current in response to doxorubicin. Next, it was found that addition of doxorubicin increased extracellular ROS over the course of 6 hours after application (Figure 4.8), in support of prior literature indicating the role of doxorubicin in redox cycling (Taymaz-Nikerel *et al.*, 2018; Songbo *et al.*, 2019; Prasanna *et al.*, 2020).

5.1. Doxorubicin treatment increases persistent Na^+ current in MDA-MB-231 cancer cells partially via CamKII

In the majority of the electrophysiological experiments, treatment of the MDA-MB-231 cells with doxorubicin resulted in an increase to the persistent Na^+ current through $Na_v1.5$ VGSCs. This is also in line with previous literature in cardiomyocytes suggesting that doxorubicin gives rise to an increased persistent Na^+ current (Cappetta *et al.*, 2017). This effect on the persistent Na^+ current was also found to occur in response to both acute application of, and pre-treatment with, doxorubicin in addition to an increase in the size of the transient Na^+ current in the acute application condition, in three out of the four experiments conducted.

Inhibiting CaMKII was the first experimental condition introduced to try and mitigate the increase to the persistent Na^+ current in response to doxorubicin. The CaMKII inhibitor KN93 partially suppressed the increase in persistent Na^+ current due to doxorubicin application. The effect, however, was not statistically significant. In cardiomyocytes, the system on which these experiments were based, increased CaMKII activation is widely accepted as playing an essential role in increasing $Na_v1.5$ VGSC activity both in cardiac dysfunctions such as arrhythmias as well as in response to doxorubicin treatment due to its ability to phosphorylate the channels at a number of sites (Wagner *et al*., 2006; Herren *et al*., 2011; Herren *et al*., 2015, Cappetta *et al*., 2017).

5.2. Doxorubicin-induced increase in persistent Na^+ current may depend on ROS but not Ca^{2+}

Ca^{2+} handling was expected to be an integral part of any mechanism underlying increased persistent Na^+ current in response to doxorubicin due to studies proposing that doxorubicin results in increases to cytosolic Ca^{2+} (Cappetta *et al*., 2017; Abdoul-Azize *et al.*, 2018; Tscheschner *et al*., 2019; Rawat *et al*., 2021). However, the experiments carried out here using both Fura-2 Ca^{2+} imaging and electrophysiology in the presence of BAPTA-AM, do not support this model. A previous study found that the direct application of 1 µM doxorubicin to MDA-MB-231 cells resulted in a robust increase to cytosolic Ca^{2+} (Abdoul-Azize *et al*. 2018). However, experiments in this thesis showed no effect of the direct application of 5 µM doxorubicin on steady state Ca^{2+} in MDA-MB-231 cells. In addition to this, experiments using CPA paired with pre-treatment with doxorubicin to assess whether doxorubicin was resulting in Ca^{2+} leakage from the intracellular stores demonstrated no significant effect of doxorubicin. This result, considered alongside the observation that BAPTA-AM did not prevent the increase to persistent Na^+ current in response to doxorubicin, suggests that altered Ca^{2+} is not necessary for doxorubicin to increase the persistent Na^+ current. However, more research is required to confirm this possibility, such as confocal microscopy experiments using Fluo-4 to look for Ca^{2+} sparks (Rizaner *et al*., 2016).

Alongside Ca^{2+}, ROS was expected to be a key factor in the mechanism underpinning an increased persistent Na^+ current in response to doxorubicin. This is due to the established ability of doxorubicin to promote redox cycling (Taymaz-Nikerel *et al*., 2018; Songbo *et al*.,

2019; Kalyanaraman., 2020; Prasanna *et al.*, 2020) as well as the capacity of ROS to sustain CaMKII activation via oxidation, something which has been reported in cardiac dysfunctions such as arrhythmias (Wagner *et al.*, 2011; Erickson., 2014; Zhao *et al.*, 2020). Results here demonstrate that doxorubicin is indeed increasing ROS in MDA-MB-231 cells, supporting what has been previously reported in cardiomyocytes (Wagner *et al.*, 2011). In addition to this, electrophysiological experiments suggested that the intracellular antioxidant Trolox may partially reduce the increase to the persistent Na^+ current in response to doxorubicin. Although the results of this experiment were not statistically significant, the treatment with Trolox was trending towards the negative control. This in conjunction with related literature (Cappetta *et al.*, 2017), suggests a potential role for ROS in this mechanism, although more work would be needed to establish the extent of this potential role.

Motility was measured as a functional output of cells treated with doxorubicin. Ptychographic imaging allowed for the tracking of both treated and untreated cells, and for the subsequent comparison of the two groups via the CellPhe app (Wilson *et al.*, 2021). This experiment demonstrated that there was a subset of doxorubicin-treated cells which appeared resistant to the drug, with a motility profile comparable to that of control cells. Interestingly, when the populations as a whole were analysed, there was an overall decrease in motility in the cells treated with doxorubicin but analysis of the treated cell population alone using K-means clustering showed that only a proportion of cells were significantly affected in terms of motility. These results are consistent with a possible functional effect of increased persistent Na^+ current through $Na_v1.5$ VGSCs, resulting in an increase to migratory behaviour in a subset of doxorubicin-resistant cells. Further work would be required to explore this possibility.

5.3. A model of doxorubicin-induced increased persistent Na^+ current

The key point of comparison for the potential mechanism underlying an increased persistent Na^+ current in MDA-MB-231 cells is the effect of doxorubicin on cardiac tissues (Cappetta *et al.*, 2017; Zhao, Zhang., 2017; Fernandez-Chas *et al.*, 2018). The results from our experiments show that, in the majority of cases, doxorubicin increases persistent Na^+ current, which fits well with previous observations in cardiomyocytes. In addition, the role of CaMKII in this mechanism is supported by CaMKII activation occurring in arrhythmias linked to increased persistent Na^+ current (Swaminathan *et al.*, 2012; Hund, Mohler., 2014).

CaMKII activation is proposed to be the mechanism by which doxorubicin alters membrane excitability in cardiomyocytes (Cappetta *et al*., 2017). This interaction between CaMKII and $Na_v1.5$ forms a possible basis for the same mechanism in MDA-MB-231 cells, where these VGSCs are present (Fraser *et al*., 2005). The possible involvement of CaMKII is small in our experiments, however, perhaps due to dilution of intracellular factors in the whole-cell patch clamp configuration because the cytosol is effectively replaced by the pipette solution. It is reported in cardiomyocytes that cardiotoxicity in response to doxorubicin is as a result of both Ca^{2+} and Na^+ overload, and that the increase in persistent Na^+ current is reliant on Ca^{2+} at least in some part (Cappetta *et al*., 2017; Fernandez-Chas *et al*., 2018). Our data did not support a requirement for Ca^{2+} in the mechanism underlying the doxorubicin-induced increase to persistent Na^+ current in MDA-MB-231 cells. However, the presence of EGTA in the patch pipette solution may mask any Ca^{2+}-dependent effect. Further experiments would be required to confirm the role (or lack thereof) of Ca^{2+}.

ROS have been implicated widely in cardiac dysfunctions such as arrhythmias as well as having the capacity to sustain CaMKII activation in such a context (Wagner *et al*., 2011; Erickson., 2014; Zhao *et al*., 2020). It has also been proposed that ROS is essential for increasing persistent Na^+ current in response to doxorubicin in cardiomyocytes (Cappetta *et al*., 2017; Fernandez-Chas *et al*., 2018). Although the effect of Trolox was not statistically significant, the trend in the data suggests that addition of an antioxidant may have prevented some of the increase in persistent Na^+ current caused by doxorubicin. These data also do not exclude the possibility that Ca^{2+} may still be required for CaMKII activation and that its oxidation via ROS may facilitate sustained activation in the absence of Ca^{2+} or following Ca^{2+}/CaM uncoupling, as has been described previously (Erickson *et al*., 2008; Erickson *et al*., 2011). With regards to the implications for migratory and invasive behaviour in doxorubicin-treated cells, it has previously been shown that treatment of MDA-MB-231 cells with doxorubicin increased migration and invasion, although this was at a much lower dose of 0.1 µM rather than the 5 µM used in our experiments (Zhong *et al*., 2017). As for our data, while there was not an increase in migratory behaviour *per se*, migration was unaffected in a subset of doxorubicin-treated cells, which is interesting due to the highly invasive and metastatic nature of the MDA-MB-231 cell line. Figure 5.1 summarises the proposed mechanism. Doxorubicin gives rise to increased ROS (and possibly Ca^{2+}) which in turn results in CaMKII activation leading to phosphorylation of $Na_v1.5$ and thus an increased persistent Na^+ current, which in turn potentially sustains migratory and invasive behaviour of

the treated cells. As for the properties of the $Na_v1.5$ channels likely affected by doxorubicin treatment, the different impacts on the transient versus persistent currents may give an indication. Given that the transient current was unchanged, doxorubicin is unlikely to affect conductance through the channel. The increased persistent Na^+ current caused by doxorubicin in the majority of experiments suggests that it is most likely to affect the slow inactivation of the channels.

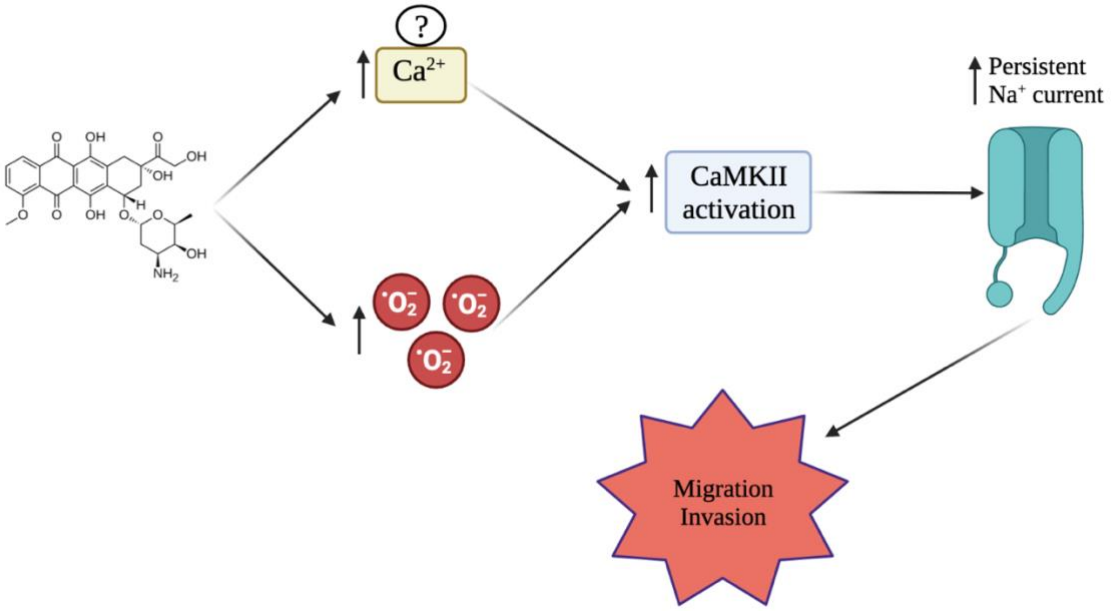

Figure 5.1 ***Schematic demonstrating a potential mechanism for doxorubicin-induced increase to persistent Na^+ current in MDA-MB-231 cells.*** *Treatment with doxorubicin results in an increase to intracellular ROS and Ca^{2+} (Cappetta* et al.*, 2017; Songbo* et al.*, 2019), resulting in increased CaMKII activation. CaMKII is capable of phosphorylating $Na_v1.5$ at a number of sites resulting in increased persistent Na^+ current (Wagner* et al.*, 2006; Herren* et al.*, 2011). This in turn can result in sustaining and/or increasing migratory and invasive behaviour in the treated cells (Yang, Brackenbury., 2013; Leslie* et al.*, 2019). Figure made with BioRender.*

5.4. Mechanistic and clinical implications of this study

Prior research has demonstrated the capacity for $Na_v1.5$ activity to promote tumorigenic behaviours, such as increased migration, in cancers where this channel is present (Yang, Brackenbury., 2012; Roger *et al*., 2015; Patel, Brackenbury., 2015; Gradek *et al*., 2019; Leslie *et al*., 2019; Luo *et al*., 2020). One such mechanism that allows for this is the altered functionality of NHE1 in the presence of an increased persistent Na^+ current. The efflux of H^+ through this transporter results in a reduced extracellular pH, ideal conditions for increased functionality of cathepsins and, in turn, the digestion of the extracellular matrix, an essential step in migratory behaviour of cancer cells (Buscoe *et* al., 2010; Brisson *et al*., 2010, Brisson *et al*., 2013; Leslie *et al*., 2019). Another such mechanism is via the reverse mode function of NCX, usually responsible for the import of Na^+ and the export of Ca^{2+}. The introduction of an increased persistent inward Na^+ current may result in the opposite, reverse mode, an efflux of Na^+ and influx of Ca^{2+} (Tykocki *et al*., 2012; Zhong *et al*., 2018; Leslie *et al*., 2019). This, as well as effects of altered membrane potential (Yang, Brackenbury., 2013), can promote the presence of 'Ca^{2+} flickers' at the leading edge of cells, further promoting migratory behaviour due to pro-migratory effects on cytoskeletal re-organisation (Ridley *et* al., 2003; Wei *et al*., 2012; Yang, Brackenbury., 2013; Tsai *et al*., 2015).

The importance of the data in this study is that treatment with doxorubicin and the resulting increase to persistent Na^+ current through $Na_v1.5$ channels has the potential to promote tumorigenic cell behaviour. If treatment with doxorubicin is resulting in increased $Na_v1.5$ channel activity in resistant cell subpopulations, this may result in the lowering of extracellular pH and increased intracellular Ca^{2+} flickers facilitating increased cell motility. This has implications for the use of anthracycline drugs in the clinical setting and highlights the importance of analysing the effects that these drugs may have on any treatment-resistant cells, potentially resulting in a more aggressive, migratory phenotype and disease recurrence. These findings also highlight the need for better, more targeted approaches for treating TNBC and approaches that improve both cancer and metastasis-free survival, as well as treatments designed more specifically for the patient and their cancer. This is no doubt an area where personalised medicine is required as the use of broad-spectrum cytotoxic drugs for the treatment of complex and patient-specific mutation-driven cancers will arguably never be as effective and may even prove ineffective in some cases. Thus, treatment with doxorubicin may be effective in the short term in reducing tumour size in the neoadjuvant setting,

however, increasing persistent Na^+ current may have the deleterious consequence of promoting migration or invasive behaviour in cells that are resistant to the cytotoxic effects of the drug. Combining doxorubicin with a VGSC blocker; e.g., ranolazine, may be necessary to mitigate the impact of pro-invasive $Na_v1.5$ channels as a result of doxorubicin treatment. This research also highlights the need to further research chemotherapeutic drugs in the context of ion channels, especially VGSCs, to mitigate or prevent any unintended pro-tumour side effects.

5.5. Limitations and Future directions

The design of these experiments come with a number of limitations and caveats. First among these is the fact that it was not proven directly that the currents measured are specifically Na^+ or that, assuming they are indeed Na^+ currents, that $Na_v1.5$ is the only carrier. Despite this, it is well established that $Na_v1.5$ is expressed in MDA-MB-231 cells (Brackenbury *et al.*, 2007) so it is highly likely that the currents measured are in fact through $Na_v1.5$ channels. With regards to the experiments blocking CaMKII with KN93, the use of whole cell patch clamping, which dilutes the cytosol with the patch pipette solution, would dilute the concentration of cytosolic CaMKII, meaning the experiments conducted may not be representative of physiological conditions in intact cells. These issues could be addressed by performing single-channel patch clamp recording to ensure only the channel of interest is being recorded as well as preventing washout of intracellular factors. This method may result in a more potent effect being demonstrated. The presence of EGTA in the patch pipette solution is also a limitation of these experiments as it means they were often carried out in nominally Ca^{2+} free conditions. This may explain why no effect of BAPTA-AM was seen on the persistent Na^+ current.

Relatively high resistance patch pipettes were used. This is due to the cells being small, so it is difficult to form giga-Ohm seals with larger low resistance pipettes. Although high resistance pipettes can result in poor voltage control, such issues were not evident in voltage dependence of activation and inactivation measurements. Series resistance compensation was also relatively low (~40%). This level was selected to avoid oscillations in cell recordings which can occur at higher levels of compensation, however, future experiments should attempt higher compensation (60-80%) if high resistance pipettes are used. Finally, the fact that the effect of doxorubicin on persistent Na^+ current was not statistically significant in the

final experiment is a concern, and would need to be addressed in future experiments. It is possible that the combination of other issues mentioned above (e.g., whole-cell recording, high series resistance, inclusion of Ca^{2+} chelator) may have contributed to a systematic under-estimation of the effect of doxorubicin on Na^{+} current.

There are several directions for further experiments to build upon this work. The first experiment studying acute doxorubicin application would have benefitted from an additional DMSO control, to exclude the possibility that low dose DMSO application could affect Na^{+} current. In addition to this, it would be useful to study the dose-dependent effect of KN93. The lack of statistical significance in the Trolox experiment, particularly for the doxorubicin-treated condition is something that stands out from the other electrophysiological experiments. This experiment would benefit from a larger number of recordings to improve statistical power. In addition, measuring motility in these cells gives a good starting point for investigating other pro-tumour behaviours such as invasion. The imaging technique used here allowed for tracking of individual cells rather than looking at the population as a whole and permitted identifying a sub-population of treatment-resistant cells. This functional output was also not constrained or limited by cell death as a result of the drug, a limitation that would hinder the use of a classical Matrigel invasion assay, for example.

Future experiments should be targeted towards further dissecting the mechanism underlying doxorubicin-induced increases to persistent Na^{+} current, e.g. by blocking multiple signalling components at once, to determine interdependence. If the mechanism in question has redundancy or the capacity for compensation, such as the interplay between ROS and Ca^{2+}, it would be beneficial to block both Ca^{2+} and ROS together, for example, via the use of both antioxidants and chelators in electrophysiological experiments. Furthermore, the Amplex red assays measure extracellular ROS whereas the mechanism behind doxorubicin mediated changes to Na^{+} current would rely on intracellular ROS, thus an assay such as Mitosox to measure mitochondrial and intracellular ROS would be beneficial (Kauffman *et al.* 2016). With regards to Ca^{2+} imaging, it is possible that the system used in our experiments was not sensitive enough to detect rapid fluxes in intracellular Ca^{2+}. Thus, the use of Fluo-4 and confocal microscopy to look for Ca^{2+} sparks (Rizaner *et al.* 2016) may be more effective for addressing the role of Ca^{2+}. Another interesting functional assay for studying cells treated with doxorubicin would be in vivo DQ-gelatin zymography to assess the invasive capacity of

the treated cells by their digestion of a fluorescent extracellular substrate (Ratnikov *et al.*, 2002). The benefit of this assay is that, similar to the ptychographic imaging used here, it does not rely on absolute cell numbers and can instead be analysed on a viable cell-by-cell basis, thus excluding the confounder of cell death. Finally, the same ptychographic imaging could be used in conjunction with VGSC blockers such as tetrodotoxin and ranolazine or via the silencing of $Na_v1.5$ using CRISPR-Cas9 (Pierre *et al.*, 2021).

5.6. Conclusions

This project has demonstrated that doxorubicin treatment increases persistent Na^+ current through $Na_v1.5$. Such an increase could have implications for behaviour of the treated cells via alterations to the extracellular pH and intracellular Ca^{2+}, leading to the promotion of a more migratory and invasive phenotype. The fact that this widely used chemotherapeutic drug can increase persistent Na^+ current, potentially leading to sustained/increased motility, invasion, and metastasis of resistant cells should be explored further. These findings also highlight the need for better, more targeted approaches to treating TNBC and approaches that improve both cancer and metastasis-free survival. Thus, combining doxorubicin with VGSC blockers may be necessary to mitigate the impact of this chemotherapeutic agent on persistent Na^+ current.

6. Acknowledgements

I would like to thank my supervisors Dr. Will Brackenbury and Dr. Sangeeta Chawla for their support throughout this project. Additional thanks go to Dr. Andy James for training me on both electrophysiology and calcium imaging, and the other members of the Brackenbury lab, with special mentions to Theo Issitt and Laura Wiggins for their help with Amplex Red assays and Livecyte imaging and CellPhe analysis, respectively.

Author's Declaration

I declare that this thesis is a presentation of original work and I am the sole author. This work has not previously been presented for an award at this, or any other, University. All sources are acknowledged as References.

7. References

Abdoul-Azize, S. *et al.* (2018) 'Integration of Ca2+ signaling regulates the breast tumor cell response to simvastatin and doxorubicin', *Oncogene*, 37(36), pp. 4979–4993.

Abdul Kadir, L., Stacey, M. and Barrett-Jolley, R. (2018) 'Emerging Roles of the Membrane Potential: Action Beyond the Action Potential', *Frontiers in physiology*, 9, p. 1661.

Agudelo, D. *et al.* (2014) 'Intercalation of antitumor drug doxorubicin and its analogue by DNA duplex: structural features and biological implications', *International journal of biological macromolecules*, 66, pp. 144–150.

Ahmed, M. *et al.* (2017) 'Modeling the human Nav1.5 sodium channel: structural and mechanistic insights of ion permeation and drug blockade', *Drug design, development and therapy*, 11, pp. 2301–2324.

Angus, M. and Ruben, P. (2019) 'Voltage gated sodium channels in cancer and their potential mechanisms of action', *Channels* , 13(1), pp. 400–409.

Arai, M. *et al.* (2000) 'Mechanism of doxorubicin-induced inhibition of sarcoplasmic reticulum Ca(2+)-ATPase gene transcription', *Circulation research*, 86(1), pp. 8–14.

Berrada, N., Delaloge, S. and André, F. (2010) 'Treatment of triple-negative metastatic breast cancer: toward individualized targeted treatments or chemosensitization?', *Annals of oncology: official journal of the European Society for Medical Oncology / ESMO*, 21 Suppl 7, pp. vii30–5.

Bong, A.H.L. *et al.* (2020) 'Assessment of doxorubicin-induced remodeling of Ca2+ signaling and associated Ca2+ regulating proteins in MDA-MB-231 breast cancer cells', *Biochemical and biophysical research communications*, 522(2), pp. 532–538.

Bouza, A.A. and Isom, L.L. (2018) 'Voltage-Gated Sodium Channel β Subunits and Their Related Diseases', *Handbook of experimental pharmacology*, 246, pp. 423–450.

Brackenbury, W.J. *et al.* (2007) 'The neonatal splice variant of Nav1.5 potentiates in vitro invasive behaviour of MDA-MB-231 human breast cancer cells', *Breast cancer research and treatment*, 101(2), pp. 149–160.

Brackenbury, W.J. (2012) 'Voltage-gated sodium channels and metastatic disease', *Channels* , 6(5), pp. 352–361.

Brackenbury, W.J. and Djamgoz, M.B.A. (2006) 'Activity-dependent regulation of voltage-gated Na+ channel expression in Mat-LyLu rat prostate cancer cell line', *The Journal of physiology*, 573(Pt 2), pp. 343–356.

Brackenbury, W.J., Djamgoz, M.B.A. and Isom, L.L. (2008) 'An emerging role for voltage-gated Na+ channels in cellular migration: regulation of central nervous system development and potentiation of invasive cancers', *The Neuroscientist: a review journal bringing neurobiology, neurology and psychiatry*, 14(6), pp. 571–583.

Brackenbury, W.J. and Isom, L.L. (2008) 'Voltage-gated Na+ channels: potential for beta subunits as therapeutic targets', *Expert opinion on therapeutic targets*, 12(9), pp. 1191–1203.

Brackenbury, W.J. and Isom, L.L. (2011) 'Na Channel β Subunits: Overachievers of the Ion Channel Family', *Frontiers in pharmacology*, 2, p. 53.

Breast cancer statistics (2015) *Cancer Research UK*. Available at: https://www.cancerresearchuk.org/health-professional/cancer-statistics/statistics-by-cancer-type/breast-cancer (Accessed: 14 June 2022).

Brisson, L. *et al.* (2011) 'Na(V)1.5 enhances breast cancer cell invasiveness by increasing NHE1-dependent H(+) efflux in caveolae', *Oncogene*, 30(17), pp. 2070–2076.

Brisson, L. *et al.* (2013) 'NaV1.5 Na^+ channels allosterically regulate the NHE-1 exchanger and promote the activity of breast cancer cell invadopodia', *Journal of cell science*, 126(Pt 21), pp. 4835–4842.

Burstein, H.J. (2022) ‘Patient education: Treatment of early HER2-positive breast cancer (Beyond the Basics)’, in D.F. Hayes and S.R. Vora (eds) *UpToDate*. Waltham, MA: UpToDate.

Busco, G. *et al.* (2010) ‘NHE1 promotes invadopodial ECM proteolysis through acidification of the peri-invadopodial space’, *FASEB journal: official publication of the Federation of American Societies for Experimental Biology*, 24(10), pp. 3903–3915.

Cappetta, D. *et al.* (2017) ‘Effects of ranolazine in a model of doxorubicin-induced left ventricle diastolic dysfunction’, *British journal of pharmacology*, 174(21), pp. 3696–3712.

Cervera, J., Alcaraz, A. and Mafe, S. (2014) ‘Membrane potential bistability in nonexcitable cells as described by inward and outward voltage-gated ion channels’, *The journal of physical chemistry. B*, 118(43), pp. 12444–12450.

Chi, M. *et al.* (2016) ‘Phosphorylation of calcium/calmodulin-stimulated protein kinase II at T286 enhances invasion and migration of human breast cancer cells’, *Scientific reports*, 6, p. 33132.

Denard, B. *et al.* (2018) ‘CREB3L1 as a potential biomarker predicting response of triple negative breast cancer to doxorubicin-based chemotherapy’, *BMC cancer*, 18(1), p. 813.

Distelmaier, F. *et al.* (2012) ‘Trolox-sensitive reactive oxygen species regulate mitochondrial morphology, oxidative phosphorylation and cytosolic calcium handling in healthy cells’, *Antioxidants & redox signaling*, 17(12), pp. 1657–1669.

Djamgoz, M.B.A., Fraser, S.P. and Brackenbury, W.J. (2019) ‘In Vivo Evidence for Voltage-Gated Sodium Channel Expression in Carcinomas and Potentiation of Metastasis’, *Cancers*, 11(11). Available at: https://doi.org/10.3390/cancers11111675.

Erickson, J.R. *et al.* (2008) ‘A dynamic pathway for calcium-independent activation of CaMKII by methionine oxidation’, *Cell*, 133(3), pp. 462–474.

Erickson, J.R. *et al.* (2011) ‘CaMKII in the cardiovascular system: sensing redox states’,

Physiological reviews, 91(3), pp. 889–915.

Erickson, J.R. (2014) 'Mechanisms of CaMKII Activation in the Heart', *Frontiers in pharmacology*, 5, p. 59.

Female Breast Cancer Subtypes - Cancer Stat Facts (no date) *SEER*. Available at: https://seer.cancer.gov/statfacts/html/breast-subtypes.html (Accessed: 27 March 2023).

Fernandez-Chas, M., Curtis, M.J. and Niederer, S.A. (2018) 'Mechanism of doxorubicin cardiotoxicity evaluated by integrating multiple molecular effects into a biophysical model', *British journal of pharmacology*, 175(5), pp. 763–781.

Fraser, S.P. *et al.* (2005) 'Voltage-gated sodium channel expression and potentiation of human breast cancer metastasis', *Clinical cancer research: an official journal of the American Association for Cancer Research*, 11(15), pp. 5381–5389.

Fraser, S.P. *et al.* (2021) 'Neonatal NaV 1.5: Pharmacological distinctiveness of a cancer-related voltage-gated sodium channel splice variant', *British journal of pharmacology* [Preprint]. Available at: https://doi.org/10.1111/bph.15668.

Gao, R. *et al.* (2009) 'Functional expression of voltage-gated sodium channels Nav1.5 in human breast cancer cell line MDA-MB-231', *Journal of Huazhong University of Science and Technology. Medical sciences = Hua zhong ke ji da xue xue bao. Yi xue Ying De wen ban = Huazhong keji daxue xuebao. Yixue Yingdewen ban*, 29(1), pp. 64–67.

Gillet, L. *et al.* (2009) 'Voltage-gated Sodium Channel Activity Promotes Cysteine Cathepsin-dependent Invasiveness and Colony Growth of Human Cancer Cells', *The Journal of biological chemistry*, 284(13), pp. 8680–8691.

Glynn, P. *et al.* (2015) 'Voltage-Gated Sodium Channel Phosphorylation at Ser571 Regulates Late Current, Arrhythmia, and Cardiac Function In Vivo', *Circulation*, 132(7), pp. 567–577.

Goldin, A.L. *et al.* (2000) 'Nomenclature of voltage-gated sodium channels', *Neuron*, 28(2), pp. 365–368.

Gradek, F. *et al.* (2019) 'Sodium Channel Nav1.5 Controls Epithelial-to-Mesenchymal Transition and Invasiveness in Breast Cancer Cells Through its Regulation by the Salt-Inducible Kinase-1', *Scientific reports*, 9(1), p. 18652.

Gustafson, T.A. *et al.* (1993) 'Mutually exclusive exon splicing of type III brain sodium channel alpha subunit RNA generates developmentally regulated isoforms in rat brain', *The Journal of biological chemistry*, 268(25), pp. 18648–18653.

Guzel, R.M. *et al.* (2019) 'Colorectal cancer invasiveness in vitro: Predominant contribution of neonatal Nav1.5 under normoxia and hypoxia', *Journal of cellular physiology*, 234(5), pp. 6582–6593.

Heinemann, S.H. *et al.* (1992) 'Calcium channel characteristics conferred on the sodium channel by single mutations', *Nature*, 356(6368), pp. 441–443.

Hegyi, B. *et al.* (2015) 'KN-93 inhibits IKr in mammalian cardiomyocytes', *Journal of molecular and cellular cardiology*, 89(Pt B), pp. 173–176.

Hempel, G. *et al.* (2002) 'Peak plasma concentrations of doxorubicin in children with acute lymphoblastic leukemia or non-Hodgkin lymphoma', *Cancer chemotherapy and pharmacology*, 49(2), pp. 133–141.

Herren, A.W. *et al.* (2011) 'CaMKII Regulates Cardiac Sodium Channel Nav1.5 by Phosphorylation in the Loop Between Domain I and II', *Biophysical journal*, 100(3), p. 421a.

Herren, A.W. *et al.* (2015) 'CaMKII Phosphorylation of Na(V)1.5: Novel in Vitro Sites Identified by Mass Spectrometry and Reduced S516 Phosphorylation in Human Heart Failure', *Journal of proteome research*, 14(5), pp. 2298–2311.

House, C.D. *et al.* (2015) 'Voltage-gated Na+ Channel Activity Increases Colon Cancer Transcriptional Activity and Invasion Via Persistent MAPK Signaling', *Scientific reports*, 5, p. 11541.

Hudis, C.A. (2007) ‘Trastuzumab--mechanism of action and use in clinical practice’, *The New England journal of medicine*, 357(1), pp. 39–51.

Hull, J.M. and Isom, L.L. (2018) ‘Voltage-gated sodium channel β subunits: The power outside the pore in brain development and disease’, *Neuropharmacology*, 132, pp. 43–57.

Hund, T.J. and Mohler, P.J. (2015) ‘Role of CaMKII in cardiac arrhythmias’, *Trends in cardiovascular medicine*, 25(5), pp. 392–397.

Hwang, K.-T. *et al.* (2018) ‘Tamoxifen therapy improves overall survival in luminal A subtype of ductal carcinoma in situ: a study based on nationwide Korean Breast Cancer Registry database’, *Breast cancer research and treatment*, 169(2), pp. 311–322.

Jiang, D. *et al.* (2020) ‘Structure of the Cardiac Sodium Channel’, *Cell*, 180(1), pp. 122–134.e10.

Jiao, Q. *et al.* (2014) ‘The latest progress in research on triple negative breast cancer (TNBC): risk factors, possible therapeutic targets and prognostic markers’, *Journal of thoracic disease*, 6(9), pp. 1329–1335.

Johnson, K.S., Conant, E.F. and Soo, M.S. (2021) ‘Molecular Subtypes of Breast Cancer: A Review for Breast Radiologists’, *Journal of Breast Imaging*, 3(1), pp. 12–24.

Johnson-Arbor, K. and Dubey, R. (2021) ‘Doxorubicin’, in *StatPearls*. Treasure Island (FL): StatPearls Publishing.

Kalyanaraman, B. (2020) ‘Teaching the basics of the mechanism of doxorubicin-induced cardiotoxicity: Have we been barking up the wrong tree?’, *Redox biology*, 29, p. 101394.

Kang, Y.J. *et al.* (2002) ‘Inhibition of doxorubicin chronic toxicity in catalase-overexpressing transgenic mouse hearts’, *Chemical research in toxicology*, 15(1), pp. 1–6.

Kauffman, M.E. *et al.* (2016) ‘MitoSOX-Based Flow Cytometry for Detecting Mitochondrial ROS’, *Reactive oxygen species (Apex, N.C.)*, 2(5), pp. 361–370.

Kellenberger, S. *et al.* (1997) ‘Molecular analysis of the putative inactivation particle in the inactivation gate of brain type IIA Na+ channels’, *The Journal of general physiology*, 109(5), pp. 589–605.

Kennecke, H. *et al.* (2010) ‘Metastatic behavior of breast cancer subtypes’, *Journal of clinical oncology: official journal of the American Society of Clinical Oncology*, 28(20), pp. 3271–3277.

Kim, D.H. *et al.* (1989) ‘Doxorubicin-induced calcium release from cardiac sarcoplasmic reticulum vesicles’, *Journal of molecular and cellular cardiology*, 21(5), pp. 433–436.

Kispersky, T.J., Caplan, J.S. and Marder, E. (2012) ‘Increase in sodium conductance decreases firing rate and gain in model neurons’, *The Journal of neuroscience: the official journal of the Society for Neuroscience*, 32(32), pp. 10995–11004.

Kruger, L.C. and Isom, L.L. (2016) ‘Voltage-Gated Na+ Channels: Not Just for Conduction’, *Cold Spring Harbor perspectives in biology*, 8(6). Available at: https://doi.org/10.1101/cshperspect.a029264.

Kümler, I. *et al.* (2016) ‘Review of hormone-based treatments in postmenopausal patients with advanced breast cancer focusing on aromatase inhibitors and fulvestrant’, *ESMO open*, 1(4), p. e000062.

Kuramoto, T. *et al.* (1981) ‘Membrane properties of a human neuroblastoma II: Effects of differentiation’, *Journal of neuroscience research*, 6(4), pp. 441–449.

Lanner, J.T. *et al.* (2010) ‘Ryanodine receptors: structure, expression, molecular details, and function in calcium release’, *Cold Spring Harbor perspectives in biology*, 2(11), p. a003996.

Lao, J. *et al.* (2013) ‘Liposomal Doxorubicin in the treatment of breast cancer patients: a review’, *Journal of drug delivery*, 2013, p. 456409.

de Lera Ruiz, M. and Kraus, R.L. (2015) ‘Voltage-Gated Sodium Channels: Structure,

Function, Pharmacology, and Clinical Indications', *Journal of medicinal chemistry*, 58(18), pp. 7093–7118.

Leslie, T.K. *et al.* (2019) 'Sodium homeostasis in the tumour microenvironment', *Biochimica et Biophysica Acta, Reviews on Cancer*, 1872(2), p. 188304.

Leslie, T.K. *et al.* (2020) 'Inhibitory Effect of Eslicarbazepine Acetate and S-Licarbazepine on Nav1.5 Channels', *Frontiers in pharmacology*, 11, p. 555047.

Lim, E. and Winer, E.P. (2011) 'Adjuvant chemotherapy in luminal breast cancers', *Breast* , 20 Suppl 3, pp. S128–31.

Liu, C.-L. *et al.* (2019) 'Doxorubicin Promotes Migration and Invasion of Breast Cancer Cells through the Upregulation of the RhoA/MLC Pathway', *Journal of breast cancer*, 22(2), pp. 185–195.

Liu, J. *et al.* (2019) 'Topoisomerase inhibitors promote cancer cell motility via ROS-mediated activation of JAK2-STAT1-CXCL1 pathway', *Journal of experimental & clinical cancer research: CR*, 38(1), p. 370.

López-Barrera, L.D. *et al.* (2020) 'Chitosan-Glutathione nanoparticles modify oxidative stress induced by doxorubicin in breast cancer cells'. Available at: https://doi.org/10.3762/bxiv.2020.24.v1.

Lopez-Charcas, O. *et al.* (2021) 'Pharmacological and nutritional targeting of voltage-gated sodium channels in the treatment of cancers', *iScience*, 24(4), p. 102270.

Lovitt, C.J., Shelper, T.B. and Avery, V.M. (2018) 'Doxorubicin resistance in breast cancer cells is mediated by extracellular matrix proteins', *BMC cancer*, 18(1), p. 41.

Lukacs, P. *et al.* (2014) 'Exploring the structure of the voltage-gated Na+ channel by an engineered drug access pathway to the receptor site for local anesthetics', *The Journal of biological chemistry*, 289(31), pp. 21770–21781.

Łukasiewicz, S. *et al.* (2021) 'Breast Cancer-Epidemiology, Risk Factors, Classification, Prognostic Markers, and Current Treatment Strategies-An Updated Review', *Cancers*, 13(17). Available at: https://doi.org/10.3390/cancers13174287.

Luo, Q. *et al.* (2020) 'The Functional Role of Voltage-Gated Sodium Channel Nav1.5 in Metastatic Breast Cancer', *Frontiers in pharmacology*, 11, p. 1111.

Lüpertz, R. *et al.* (2010) 'Dose- and time-dependent effects of doxorubicin on cytotoxicity, cell cycle and apoptotic cell death in human colon cancer cells', *Toxicology*, 271(3), pp. 115–121.

Mao, W. *et al.* (2012) 'Reactive oxygen species suppress cardiac NaV1.5 expression through Foxo1', *PloS one*, 7(2), p. e32738.

Mao, W. *et al.* (2019) 'The Emerging Role of Voltage-Gated Sodium Channels in Tumor Biology', *Frontiers in oncology*, 9, p. 124.

Marchal, G.A. *et al.* (2020) 'The sodium channel NaV 1.5 impacts on early murine embryonic cardiac development, structure and function in a non-electrogenic manner', *Acta physiologica* , 230(2), p. e13493.

Marinello, P.C. *et al.* (2019) 'Metformin prevention of doxorubicin resistance in MCF-7 and MDA-MB-231 involves oxidative stress generation and modulation of cell adaptation genes', *Scientific reports*, 9(1), p. 5864.

Martínez-Sáez, O. and Prat, A. (2021) 'Current and Future Management of HER2-Positive Metastatic Breast Cancer', *JCO oncology practice*, 17(10), pp. 594–604.

Matasic, D.S. *et al.* (2020) 'Modulation of the cardiac sodium channel NaV1.5 peak and late currents by NAD+ precursors', *Journal of molecular and cellular cardiology*, 141, pp. 70–81.

Nabieva, N. and Fasching, P.A. (2021) 'Endocrine Treatment for Breast Cancer Patients Revisited-History, Standard of Care, and Possibilities of Improvement', *Cancers*, 13(22). Available at: https://doi.org/10.3390/cancers13225643.

Narahashi, T. (1974) ‘Chemicals as tools in the study of excitable membranes’, *Physiological reviews*, 54(4), pp. 813–889.

Nelson, M. *et al.* (2014) ‘The sodium channel β1 subunit mediates outgrowth of neurite-like processes on breast cancer cells and promotes tumour growth and metastasis’, *International journal of cancer. Journal international du cancer*, 135(10), pp. 2338–2351.

Nelson, M., Yang, M., Millican-Slater, R., *et al.* (2015) ‘Nav1.5 regulates breast tumor growth and metastatic dissemination in vivo’, *Oncotarget*, 6(32), pp. 32914–32929.

Nelson, M., Yang, M., Dowle, A.A., *et al.* (2015) ‘The sodium channel-blocking antiepileptic drug phenytoin inhibits breast tumour growth and metastasis’, *Molecular cancer*, 14, p. 13.

Onkal, R. *et al.* (2008) ‘Alternative splicing of Nav1.5: an electrophysiological comparison of “neonatal” and “adult” isoforms and critical involvement of a lysine residue’, *Journal of cellular physiology*, 216(3), pp. 716–726.

Onkal, R. and Djamgoz, M.B.A. (2009) ‘Molecular pharmacology of voltage-gated sodium channel expression in metastatic disease: clinical potential of neonatal Nav1.5 in breast cancer’, *European journal of pharmacology*, 625(1-3), pp. 206–219.

Onkal, R., Fraser, S.P. and Djamgoz, M.B.A. (2019) ‘Cationic Modulation of Voltage-Gated Sodium Channel (Nav1.5): Neonatal Versus Adult Splice Variants-1. Monovalent (H+) Ions’, *Bioelectricity*, 1(3), pp. 139–147.

Patel, F. and Brackenbury, W.J. (2015) ‘Dual roles of voltage-gated sodium channels in development and cancer’, *The International journal of developmental biology*, 59(7-9), pp. 357–366.

Pchelintseva, E. and Djamgoz, M.B.A. (2018) ‘Mesenchymal stem cell differentiation: Control by calcium-activated potassium channels’, *Journal of cellular physiology*, 233(5), pp. 3755–3768.

Pettit, E.J. and Fay, F.S. (1998) ‘Cytosolic free calcium and the cytoskeleton in the control of leukocyte chemotaxis’, *Physiological reviews*, 78(4), pp. 949–967.

Pierre, M. *et al.* (2021) ‘NaV1.5 knockout in iPSCs: a novel approach to study NaV1.5 variants in a human cardiomyocyte environment’, *Scientific reports*, 11(1), p. 17168.

Pilco-Ferreto, N. and Calaf, G.M. (2016) ‘Influence of doxorubicin on apoptosis and oxidative stress in breast cancer cell lines’, *International journal of oncology*, 49(2), pp. 753–762.

Prasanna, P.L., Renu, K. and Valsala Gopalakrishnan, A. (2020) ‘New molecular and biochemical insights of doxorubicin-induced hepatotoxicity’, *Life sciences*, 250, p. 117599.

Ratnikov, B.I., Deryugina, E.I. and Strongin, A.Y. (2002) ‘Gelatin zymography and substrate cleavage assays of matrix metalloproteinase-2 in breast carcinoma cells overexpressing membrane type-1 matrix metalloproteinase’, *Laboratory investigation; a journal of technical methods and pathology*, 82(11), pp. 1583–1590.

Rawat, P.S. *et al.* (2021) ‘Doxorubicin-induced cardiotoxicity: An update on the molecular mechanism and novel therapeutic strategies for effective management’, *Biomedicine & pharmacotherapy = Biomedecine & pharmacotherapie*, 139, p. 111708.

Ridley, A.J. *et al.* (2003) ‘Cell migration: integrating signals from front to back’, *Science*, 302(5651), pp. 1704–1709.

Rizaner, N. *et al.* (2016) ‘Intracellular calcium oscillations in strongly metastatic human breast and prostate cancer cells: control by voltage-gated sodium channel activity’, *European biophysics journal: EBJ*, 45(7), pp. 735–748.

Rodriguez-Mora, O. *et al.* (2006) ‘Inhibition of the CaM-Kinases augments cell death in response to oxygen radicals and oxygen radical inducing cancer therapies in MCF-7 human breast cancer cells’, *Cancer biology & therapy*, 5(8), pp. 1022–1030.

Roger, S. *et al.* (2015) ‘Voltage-gated sodium channels and cancer: is excitability their

primary role?', *Frontiers in pharmacology*, 6, p. 152.

Roger, S., Besson, P. and Le Guennec, J.-Y. (2003) 'Involvement of a novel fast inward sodium current in the invasion capacity of a breast cancer cell line', *Biochimica et biophysica acta*, 1616(2), pp. 107–111.

Rohl, C.A. *et al.* (1999) 'Solution structure of the sodium channel inactivation gate', *Biochemistry*, 38(3), pp. 855–861.

Rokhlin, O. *et al.* (2010) 'KN-93 inhibits androgen receptor activity and induces cell death irrespective of p53 and Akt status in prostate cancer', *Cancer biology & therapy*, 9(3), pp. 224–234.

Saeki, K. *et al.* (2002) 'Doxorubicin directly binds to the cardiac-type ryanodine receptor', *Life sciences*, 70(20), pp. 2377–2389.

Sarao, R. *et al.* (1991) 'Developmentally regulated alternative RNA splicing of rat brain sodium channel mRNAs', *Nucleic acids research*, 19(20), pp. 5673–5679.

Schwab, A. *et al.* (2012) 'Role of ion channels and transporters in cell migration', *Physiological reviews*, 92(4), pp. 1865–1913.

Singh, D.D., Parveen, A. and Yadav, D.K. (2021) 'Role of PARP in TNBC: Mechanism of Inhibition, Clinical Applications, and Resistance', *Biomedicines*, 9(11). Available at: https://doi.org/10.3390/biomedicines9111512.

Slamon, D.J. *et al.* (2001) 'Use of chemotherapy plus a monoclonal antibody against HER2 for metastatic breast cancer that overexpresses HER2', *The New England journal of medicine*, 344(11), pp. 783–792.

Song, W. and Shou, W. (2012) 'Cardiac sodium channel Nav1.5 mutations and cardiac arrhythmia', *Pediatric cardiology*, 33(6), pp. 943–949.

Song, Y. *et al.* (2006) 'Blocking late sodium current reduces hydrogen peroxide-induced

arrhythmogenic activity and contractile dysfunction', *The Journal of pharmacology and experimental therapeutics*, 318(1), pp. 214–222.

Songbo, M. *et al.* (2019) 'Oxidative stress injury in doxorubicin-induced cardiotoxicity', *Toxicology letters*, 307, pp. 41–48.

Sumi, M. *et al.* (1991) 'The newly synthesized selective Ca2+/calmodulin dependent protein kinase II inhibitor KN-93 reduces dopamine contents in PC12h cells', *Biochemical and biophysical research communications*, 181(3), pp. 968–975.

Sundelacruz, S., Levin, M. and Kaplan, D.L. (2008) 'Membrane potential controls adipogenic and osteogenic differentiation of mesenchymal stem cells', *PloS one*, 3(11), p. e3737.

Swaminathan, P.D. *et al.* (2012) 'Calmodulin-dependent protein kinase II: linking heart failure and arrhythmias', *Circulation research*, 110(12), pp. 1661–1677.

Taymaz-Nikerel, H. *et al.* (2018) 'Doxorubicin induces an extensive transcriptional and metabolic rewiring in yeast cells', *Scientific reports*, 8(1), p. 13672.

Tsai, F.-C. *et al.* (2015) 'Ca2+ signaling in cytoskeletal reorganization, cell migration, and cancer metastasis', *BioMed research international*, 2015, p. 409245.

Tscheschner, H. *et al.* (2019) 'CaMKII activation participates in doxorubicin cardiotoxicity and is attenuated by moderate GRP78 overexpression', *PloS one*, 14(4), p. e0215992.

Tykocki, N.R., Jackson, W.F. and Watts, S.W. (2012) 'Reverse-mode Na+/Ca2+ exchange is an important mediator of venous contraction', *Pharmacological research: the official journal of the Italian Pharmacological Society*, 66(6), pp. 544–554.

Uchida, N., Suda, T. and Ishiguro, K. (2013) 'Effect of chemotherapy for luminal a breast cancer', *Yonago acta medica*, 56(2), pp. 51–56.

Vargas, E. *et al.* (2012) 'An emerging consensus on voltage-dependent gating from computational modeling and molecular dynamics simulations', *The Journal of general*

physiology, 140(6), pp. 587–594.

Wagner, S. *et al.* (2006) ‘Ca2+/calmodulin-dependent protein kinase II regulates cardiac Na+ channels’, *The Journal of clinical investigation*, 116(12), pp. 3127–3138.

Wagner, S. *et al.* (2011) ‘Reactive oxygen species-activated Ca/calmodulin kinase IIδ is required for late I(Na) augmentation leading to cellular Na and Ca overload’, *Circulation research*, 108(5), pp. 555–565.

Wahba, H.A. and El-Hadaad, H.A. (2015) ‘Current approaches in treatment of triple-negative breast cancer’, *Cancer biology & medicine*, 12(2), pp. 106–116.

Wang, J., Ou, S.-W. and Wang, Y.-J. (2017) ‘Distribution and function of voltage-gated sodium channels in the nervous system’, *Channels* , 11(6), pp. 534–554.

Wang, Q. *et al.* (2021) ‘CaMKII oxidation is a critical performance/disease trade-off acquired at the dawn of vertebrate evolution’, *Nature communications*, 12(1), p. 3175.

Ward, C.A. and Giles, W.R. (1997) ‘Ionic mechanism of the effects of hydrogen peroxide in rat ventricular myocytes’, *The Journal of physiology*, 500 (Pt 3), pp. 631–642.

Wei, C. *et al.* (2012) ‘Calcium gradients underlying cell migration’, *Current opinion in cell biology*, 24(2), pp. 254–261.

Wenningmann, N. *et al.* (2019) ‘Insights into Doxorubicin-induced Cardiotoxicity: Molecular Mechanisms, Preventive Strategies, and Early Monitoring’, *Molecular pharmacology*, 96(2), pp. 219–232.

West, J.W. *et al.* (1992) ‘A cluster of hydrophobic amino acid residues required for fast Na(+)-channel inactivation’, *Proceedings of the National Academy of Sciences of the United States of America*, 89(22), pp. 10910–10914.

Wilson, J.C. *et al.* (2021) ‘CellPhe: a toolkit for cell phenotyping using time-lapse imaging and pattern recognition’, *Research Square*. Available at: https://doi.org/10.21203/rs.3.rs-

971415/v1.

Wong, M.H. *et al.* (2019) 'The KN-93 Molecule Inhibits Calcium/Calmodulin-Dependent Protein Kinase II (CaMKII) Activity by Binding to Ca2+/CaM', *Journal of molecular biology*, 431(7), pp. 1440–1459.

Xu, L. *et al.* (2019) 'Voltage-gated sodium channels: structures, functions, and molecular modeling', *Drug discovery today*, 24(7), pp. 1389–1397.

Yamaci, R.F. *et al.* (2017) 'Neonatal Nav1.5 protein expression in normal adult human tissues and breast cancer', *Pathology, research and practice*, 213(8), pp. 900–907.

Yang, F. *et al.* (2014) 'Doxorubicin, DNA torsion, and chromatin dynamics', *Biochimica et biophysica acta*, 1845(1), pp. 84–89.

Yang, M. and Brackenbury, W.J. (2013) 'Membrane potential and cancer progression', *Frontiers in physiology*, 4, p. 185.

Yersal, O. and Barutca, S. (2014) 'Biological subtypes of breast cancer: Prognostic and therapeutic implications', *World journal of clinical oncology*, 5(3), pp. 412–424.

Yin, L. *et al.* (2020) 'Triple-negative breast cancer molecular subtyping and treatment progress', *Breast cancer research: BCR*, 22(1), p. 61.

Yu, F.H. and Catterall, W.A. (2003) 'Overview of the voltage-gated sodium channel family', *Genome biology*, 4(3), p. 207.

Zhang, P. (2017) 'CaMKII: The molecular villain that aggravates cardiovascular disease', *Experimental and therapeutic medicine*, 13(3), pp. 815–820.

Zhang, W. *et al.* (2012) 'IP3-dependent intracellular Ca2+ release is required for cAMP-induced c-fos expression in hippocampal neurons', *Biochemical and biophysical research communications*, 425(2), pp. 450–455.

Zhang, Y. *et al.* (2014) ‘Doxorubicin induces sarcoplasmic reticulum calcium regulation dysfunction via the decrease of SERCA2 and phospholamban expressions in rats’, *Cell biochemistry and biophysics*, 70(3), pp. 1791–1798.

Zhao, L. and Zhang, B. (2017) ‘Doxorubicin induces cardiotoxicity through upregulation of death receptors mediated apoptosis in cardiomyocytes’, *Scientific reports*, 7, p. 44735.

Zhao, N. *et al.* (2020) ‘Role of Oxidation-Dependent CaMKII Activation in the Genesis of Abnormal Action Potentials in Atrial Cardiomyocytes: A Simulation Study’, *BioMed research international*, 2020, p. 1597012.

Zhong, X. *et al.* (2018) ‘Reverse mode of sodium/calcium exchanger subtype 1 contributes to detrusor overactivity in rats with partial bladder outflow obstruction’, *American journal of translational research*, 10(3), pp. 806–815.

Zhong, Z.-F. *et al.* (2017) ‘Combined effects of furanodiene and doxorubicin on the migration and invasion of MDA-MB-231 breast cancer cells in vitro’, *Oncology reports*, 37(4), pp. 2016–2024.